# A STUDY OF THE X-RAY EMISSION FROM THREE RADIO PULSARS

NASA Grant NAG5-2329

Annual Report No. 2 & 3

For the Period 1 February 1994 through 31 January 1996

Principal Investigator
Dr. Patrick O. Slane

April 1996

Prepared for:

National Aeronautics and Space Administration
Goddard Space Flight Center
Greenbelt, Maryland 20771

Smithsonian Institution
Astrophysical Observatory
Cambridge, Massachusetts 02138

The Smithsonian Astrophysical Observatory
is a member of the
Harvard-Smithsonian Center for Astrophysics

The NASA Technical Officer for this grant is Dr. Robert Petre, Code 666, Laboratory for High Energy Astrophysics, Space Science Directorate, Goddard Space Flight Center, Greenbelt, Maryland 20771.

The subject grant is for work on a study of x-ray emission from isolated pulsars. The purpose of the study was to 1) determine whether the pulsars were x-ray sources; and, if so, 2) search for evidence of pulsations at the known radio period; and 3) study the nature of the x-ray emission.

I obtained a ~20 ks PSPC observation of the pulsar PSR 0355+54, and the analysis of these data is complete. These results were reported at the 183rd AAS Meeting, and in a paper entitled "X-Ray Emission from PSR 0355+54" which was published in the *The Astrophysical Journal.*

I also obtained a ~ 3 ks PSPC observations of PSR 1642-03. A summary of the results from these data were reported in a Conference Proceedings for the "New Horizon of X-ray Astronomy" symposium. In addition, as part of a study with a student from the SAO Summer Intern Program, I incorporated ROSAT archival data in an extended study of pulsar emission. These results were reported at the 185th AAS Meeting, and in a paper entitled "Soft X-ray Emission from Selected Isolated Pulsars" which was published in *The Astrophysical Journal (Letters).*

I have included copies of these papers to serve as the annual report on this project.

37.11

**Pulse and Polarization Morphology for $\gamma$-Ray Pulsars**

Roger W. Romani & I.-A. Yadigaroglu (Stanford University)

The location and efficiency of pulsar $\gamma$-ray emission is a subject of appreciable debate. The variety of profiles found in recent EGRET detections motivates improved modeling. We present a calculation of polarization and profile properties of high energy pulsar emission in an outer gap picture. Our sums indicate that comparison with the polarization data and with radio pulse profiles provides significant constraints on the emission zone geometry. We find that high energy emission is generally detected from the pole opposite that associated with the surface radio pulse; the result is robust to uncertainties in the outer magnetosphere currents and details of the field geometry. The Crab pulsar provides an important test case and we match the model to optical polarization measurements tracing the outer gap region, as well as the high energy light curves. With spin axis inclinations and viewing geometries provided by the model fit, we derive an effective beaming factor that can be used to estimate the total flux from the detected value. We also show that this picture provides good correspondence to the $\gamma$-ray light curves and radio pulse offset and polarization properties for the other $\gamma$-ray pulsars (*e.g.* PSR 1706-44, Geminga) and provides useful constraints on the emission altitude; these provide a clue to the origin of the spectral index variations in the $\gamma$-ray data.

37.12

**X-Ray Emission From PSR 0355+54**

Patrick Slane (CfA)

We have obtained a 20 ks observation of PSR 0355+54 using the ROSAT PSPC. The pulsar is detected with a count rate of $4.4(\pm 1.4) \times 10^{-3}$ s above the background. While the $\sim$ 85 source counts are insufficient for spectral fitting, we have derived source parameters for the cases of power law as well as blackbody spectra. For a Crab-like spectrum (photon index $\alpha = 2$) we find $L_x(0.1 - 2.4 \text{ keV}) = 8.0 \times 10^{31}$ erg s$^{-1}$, somewhat higher than upper limits reported from Einstein observations but consistent with typical $L_x$ vs $\dot{E}$ values for other pulsars. For blackbody emission, we derive a temperature upper limit of $\sim 10^6$ K for emission from the entire neutron star surface, which is consistent with standard models for cooling of the neutron star interior given a characteristic age $10^{5.75}$ y. No evidence is revealed for modulation at the 0.156 s pulsar period, setting an upper limit of $\sim$ 25% for the pulsed fraction of the x-ray signal.

37.13

**A Possible EXOSAT Detection of the Hard X-ray Transient GRO J1008-57**

D.J. Macomb and C.R. Shrader (NASA/CSC)

The BATSE experiment onboard the Gamma-Ray Observatory recently detected a new, hard, x-ray pulsar given the name GRO J1008-57 with a pulsation period of 93.587+/-0.005 seconds (Stollberg, et.al., IAU Circular 5838). A ROSAT PSPC observation with positional uncertainty of 15" determined the location of the x-ray source to be, in J2000 coordinates, R.A. = 10h09m46s, Decl. = -58deg17'32" (Petre & Gehrels, IAU Circular 5877). A search of the EXOSAT archives shows that a 1985 observation centered on HD 88661 with both the ME detector (field of view 0.75x0.75 degrees) and CMA detector (2x2 degrees), centered at a pointing position only 0.35 degrees away from the ROSAT location, includes GRO J1008-57 in the field-of-view. We present evidence for the detection of an x-ray pulsation period of 91.37+/-0.08 seconds in the 0.8-3.9 keV band of the ME instrument. Additionally, we present arguments against stellar coronal emission or other serendipitous sources being responsible for the ME flux. If our interpretation of the data is correct, the mean period derivative of the source is $2.7x10^{-3}yr^{-1}$ and its nominal quiescent flux is $1.1x10^{-11}ergscm^{-2}s^{-1}$. Implications for possible physical system parameters are discussed. Finally, several possible optical counterparts are identified and discussed.

## Session 38: Supernovae
## Display Session
## Salons I/II

38.01

**The Deceleration Parameter from SN Ia Photometry?**

Thomas E. Vaughan and David Branch (U. of Okla. Phys. & Astr.)

In order to investigate the feasibility of determining the cosmic deceleration parameter from high redshift ($z = 0.5 \rightarrow 1.5$) type Ia supernova photometry alone, a representative time-evolving spectrum is constructed from 19 UV and optical spectra of SN 1992A and SN 1981B. By K-correcting and time-dilating this "spectral surface," we approximate the evolution of light curves and colors with redshift. Assuming that the SN Ia production rate is constant in time and space, we find, for $q_o = 0.5$, that a single 8'×8' field (as in the Omega Telescope proposal, Pennypacker et al., 1993) has about one SN Ia per year out to z = 1.5. We estimate the observable fraction of these supernovae as a function of limiting magnitude.

38.02

**The Type Ia Supernovae in IC 4182 and NGC 5253 and the Value of the Hubble Constant**

Peter Nugent, Adam Fisher and David Branch (University of Oklahoma, Department of Physics and Astronomy)

Sandage et al. have used the HST to determine the Cepheid-based distances to IC 4182, the parent galaxy of the Type Ia supernova 1937C, and to NGC 5253, the parent galaxy of the Type Ia supernovae 1972E and 1895B. We compare the spectroscopic and photometric properties of these three calibrator supernovae with the properties of more distant Type Ia supernovae and derive a low value of the Hubble constant.

38.03

**The Hubble Constant from Nickel Radioactivity in Type Ia Supernovae**

Adam Fisher, David Branch, Peter Nugent (Dept of Physics and Astronomy, University of Oklahoma)

On the assumptions that Type Ia supernovae are thermonuclear disruptions of carbon-oxygen white dwarfs near the Chandrasekhar mass and that their light curves are powered by nickel and cobalt decay, the characteristic SN Ia peak luminosity can be estimated provided that the ejected nickel mass is known. We use spectrum analysis and a simple analytic model to obtain an improved estimate of the nickel mass. The resulting luminosity estimate, combined with the observational Hubble diagram for SNe Ia, requires a low value of the Hubble constant.

38.04

**Type II Supernova Light Curves: Influence of the He Core Mass**

T. R. Young, E. Baron, and D. Branch (University of Oklahoma)

A study of numerical Type II supernova light curves showing the effects of various helium core masses is carried out. The simulations use a 1-dimensional, flux-limited hydrodynamical code which accesses opacity tables and accounts for gamma ray deposition. Presupernova models used in this study have helium core masses of about 2, 3, 4, 6, and 8 $M_\odot$, taken from calculations by Nomoto and Woosley. The hydrogen envelope is modified by homologous transformations to vary its radius and mass. The influence of the helium core mass on the shape and absolute magnitude of the light curve is shown independent of other parameters that affect the light curve.

# ROSAT OBSERVATIONS OF PSR 0355+54 and PSR 1642–03

Patrick Slane
Harvard-Smithsonian Center for Astrophysics
60 Garden Street, Cambridge, MA 02138
USA

ABSTRACT

PSR 0355+54 and PSR 1642–03 are both radio pulsars whose X-ray behavior was left unresolved by *Einstein* observations.[1,2] In each case, faint emission was detected near the sources, but appeared to be concentrated 1–2 arcmin from the known pulsar positions. This was interpreted as evidence of either extended emission or of the presence of a serendipitous background object. We have carried out ROSAT PSPC observations of these two pulsars to determine the nature of the emission; here we report on the results of preliminary analysis.

## 1. Introduction

PSR 0355+54 is a moderate age pulsar ($T_{\rm char} = 10^{5.75}$ y) with a fairly short period (156 ms). The primary properties determined from radio observations[3] are summarized below:

| PSR | $P$ (s) | $\dot{P}/10^{-15}$ ( s s$^{-1}$) | $\log \dot{E}$ (ergs s$^{-1}$) | $\log T$ (years) | DM (cm$^{-3}$ pc) | D (kpc) | $\log B$ (Gauss) |
|---|---|---|---|---|---|---|---|
| 0355+54 | 0.156 | 4.4 | 34.66 | 5.75 | 57 | 2.07 | 11.92 |
| 1055–52 | 0.197 | 5.8 | 34.48 | 5.73 | 30 | 1.53 | 12.04 |
| 1642–03 | 0.388 | 1.8 | 33.08 | 6.54 | 36 | 2.90 | 11.93 |

Using the spin-down energy loss rate as an indicator, PSR 0355+54 is a good candidate for observable X-ray emission; only 10 of the 119 radio pulsars closer than PSR 0355+54 have larger values of $\dot{E}/D^2$, and 8 of these are known X-ray emitters. Observations carried out with the *Einstein* Observatory were inconclusive, however. Weak emission from a position $\sim 1.7$ arcmin from the radio position was detected, which was interpreted as possible evidence of extended emission from an associated synchrotron nebula.[1] The similarity between this pulsar and PSR 1055–52 (see Table above), which is a known X-ray source[4,5] and has been recently detected as a $\gamma$-ray source[6], makes further study particularly interesting.

*Einstein* studies of PSR 1642–03 provided results similar to those for PSR 0355+54; faint emission concentrated $\sim 1$ arcmin from the pulsar position was observed, and this was interpreted as possible evidence for an extended synchrotron nebula.[1] The derived luminosity[2] $L_x = 8.5 \times 10^{31}$ ergs s$^{-1}$ is very high given the available spin-down power (see Table above). Assuming the emission is actually associated with the pulsar, this suggests either a particularly efficient mechanism for converting $\dot{E}$ into X-rays, or the presence of an additional energy source. Cooling of the neutron star interior does not seem a viable interpretation, however, given the age of the pulsar. Further study is thus of interest to determine whether the emission is actually associated with the pulsar and what implications the large luminosity may have for emission models as well as for detectability of other pulsars with moderate values of $\dot{E}$.

## 2. ROSAT Observations

PSR 0355+54 was observed for 19,144 s using the ROSAT Position Sensitive Proportional Counter (PSPC). After cleaning, 16,644 s of good data remain for analysis; here we present a summary of the results from the full analysis.[7] A faint X-ray source is detected at the position of the radio pulsar with a count rate $R = 4.2(\pm 1.3) \times 10^{-3}$ s$^{-1}$. We have smoothed the image with a 32 arcsec Gaussian smoothing scale, and subtracted a scaled and similarly

NEW HORIZON OF X-RAY ASTRONOMY
—first results from ASCA—

smoothed point source for the PSPC to reveal weak residual emission concentrated $\sim 1.6$ arcmin from the pulsar, in the northeast. Inspection of the surrounding PSPC field reveals a number of similar weak sources, suggesting that this emission is likely to be associated with a background source rather than from an extended pulsar component. We have searched for pulsations at the known radio period of 156 ms but find no evidence using all data (61 counts) from a 30 arcsec circle centered on the point source. Given the small number of counts, this is not surprising; the null detection permits us to establish a $3\sigma$ upper limit $f < 77\%$. Most pulsars have pulsed fractions smaller than this. PSR 1055–52 has $f \sim 85\%$ at higher energies, but a corresponding effect would not be seen for PSR 0355+54 due to lack of photons.

With only $\sim 70$ counts, there is not sufficient information to perform spectral model fitting. Instead, we have considered two cases: 1)a Crab-like power law which might be associated with magnetospheric emission; and 2)blackbody emission from the entire surface of the neutron star (NS), which could result from cooling of the NS interior. By using hardness ratios defined in the standard processing of PSPC spectral data, we have compared the observed spectrum with that predicted by model spectra convolved through the telescope spectral response. Assuming a column density $N_H = 3 \times 10^{21}$ cm$^{-2}$ (derived by scaling the Crab value by the ratio of DM values) we find a surface temperature $T = 1.33(\pm 0.07) \times 10^6$ K (corrected for gravitational redshift) is required to reproduce the PSPC count rate. This temperature is consistent with predictions from current cooling models. However, we find that models for emission from the entire surface of a NS with $R = 10$ km are unable to reproduce the observed hardness ratios, and are particularly poor representations for any reasonable values of $N_H$. We conclude that the emission is not associated with cooling of the NS interior; rather, it is derived from the pulsar spin-down. This does not rule out the possibility of blackbody emission at a higher temperature, from smaller regions on the NS surface. Such a scenario could result from bombardment of the polar caps by energetic particles accelerated in the pulsar magnetosphere. A Crab-like spectrum power-law spectrum ($\alpha = 2$) yields $L_x(0.1-2.4\ \mathrm{keV}) = 8.0 \times 10^{31}$ ergs s$^{-1}$, consistent with observed luminosities for other pulsars. In particular, it is very similar to that derived for the power-law component from PSR 1055–52.[7] This similarity suggests that PSR 0355+54 is a good candidate for $\gamma$-ray observations.

Our scheduled 40 ks observation of PSR 1642-03 was cut short to $\sim 3$ ks. Emission from the vicinity of the pulsar is clearly detected, but as in the *Einstein* data the emission is offset from the pulsar position. The shortened observation yielded only $\sim 35$ counts, insufficient to assess whether the emission is associated with the pulsar or a background source. Using a Crab-like power law spectrum with $N_H = 1.5 \times 10^{21}$ cm$^{-2}$, scaled from the Crab-value, the observed count rate would indicate a pulsar luminosity $L_x(0.1-2.4\ \mathrm{keV}) \sim 2 \times 10^{32}$ ergs s$^{-1}$. This is extremely large relative to other pulsars given the spin-down energy $\dot{E} = 1.2 \times 10^{33}$ ergs s$^{-1}$. If correct, the result has strong implications relative to the emission mechanisms. PSR 1642–03 proper motion measurements indicate large velocity ($\sim 660$ km s$^{-1}$) directed $\sim 30°$ south of east - in reasonable agreement with the direction of the emission. Models for synchrotron emission from a ram-pressure confined wind[8] may explain the offset emission; luminosity values appear problematic, however. Further analysis of this interpretation is in progress.

## 3. References

1. Helfand, D.J. 1983, Proc. IAU Symp. 101, ed. J. Danzinger and P. Gorenstein p.471
2. Seward, F. D., & Wang, Z-R 1988, ApJ, 332, 199
3. Taylor, J. H., Manchester, R. N., & Lyne, A. G. 1993, ApJ Supp., 88, 529
4. Cheng, A. F., & Helfand, D. J. 1983, ApJ, 217, 271
5. Ögelman, H., & Finley, J. P. 1993, ApJ, 413, L31
6. Fierro, J. M. *et al.* 1993, ApJ, 413, L27
7. Slane, P. 1994, ApJ, submitted.
8. Cheng, A. F. 1983, ApJ, 275, 790

"blob." Use of a subset of the particles removes the overlap but also throws away information about the simulation via an increase in random noise or granularity. The point overlap problem is overcome by using different degrees of shading or color to represent the increasing number of particles per unit area rather than plotting them individually. The particle numbers are computed in individual bins of a cartesian grid typically of 256x256 cells providing good resolution of features.

However, simple bin number densities do not solve all display problems. Even with the particle numbers possible today, simulations do not contain "billions of stars." Consequently, the particles are so sparsely distributed in the intermediate and outer regions that there is considerable random noise or they are even seen individually in bins. To solve this problem, the color/density method must be made more sophisticated. We discuss methods of creating a smoothed number density over the simulation disk which approximates the particle density distribution if billions of particles had been used. The smoothing method only displays peaks or valleys in the particle distribution if they exceed a chosen level of statistical significance. Display of number density via shading or color along with a smoothing method which judges the significance of a feature permits use of the quantitative techniques observers have developed for CCD images to be used on simulations also. Finally! , when the smoothing and shading is done, the final image is more esthetically pleasing!

This work was supported by NSF grants REU AST 9300413, EPSCoR RII8996152 and AST 9014137.

77.20

**Sticky Particle Simulations of Counterrotating Disk Formation**

A.R.Thakar, B.S.Ryden (Ohio State U.)

Extensive counterrotating disks seen in spirals/S0s in recent years pose a challenge to theorists. Adiabatic, dissipational infall of ambient gas in a retrograde orbit around the disk is thought to be the most likely mechanism for the formation of such disks. We present results of sticky particle simulations of this process. We find that gas which is constrained to move in a retrograde orbit around the disk and loses kinetic energy in cloud-cloud collisions settles into the plane of the disk and forms a counterrotating gas disk within a fraction of a Hubble time. The mass of the infalling gas is critical to the stability of the disk, and the gas must fall in a little at a time to avoid disruption of the disk. Dissipationless infall is unable to produce counterrotating disks because the material does not settle into the disk plane within a Hubble time. The initial angular momentum of the infalling gas determines the time-scale of the counterrotating disk formation for the most part.

## Session 78: Pulsars and Neutron Stars
## Display Session, 9:20am - 6:30pm
## Tucson Convention Center, Exhibit Hall A

78.01

**UV-Optical Observations of Pulsars with post-COSTAR HST**

G. S. Stringfellow, G. G. Pavlov, & F. A. Córdova (The Pennsylvania State University)

We have carried out post-COSTAR HST observations with the FOC/96 to search for UV and optical emission from 3 nearby pulsars (PSR 0656+14, PSR 0950+08, and PSR 1929+10) spanning a range in age between $1\times10^5-2\times10^7$ years. All three pulsars were observed with the F130LP filter, and for PSR 1929+10 observations were also obtained for the F342W (U-band) and F430W (B-band) filters. Probable candidates have been detected and count rates determined. The count rates exceed by several orders of magnitude those expected from thermal radiation emitted at the surface of the neutron star, as estimated from *ROSAT* observations. This radiation must therefore be of a non-thermal origin, and its intensity greatly exceeds predictions of existing phenomenological models. Non-thermal radiation appears to be a more common property of older pulsars than heretofore believed.

78.02

**Resolving Pulsar Magnetospheres Using Interstellar Scintillation**

T. V. Smirnova, V. I. Shishov, V. M. Malofeev (Lebedev Physical Inst.)

Pulsars exhibit variations or scintillation of radio emission in time and frequency caused by electron density inhomogeneities of the interstellar medium. Two sources with transverse separation more than the size of the diffracton pattern at the Earth will produce independent scintillations from these sources. We used this idea to resolve pulsar magnetospheres. Here we present new observations of 3 pulsars — PSR 0834+6, 1133+16, and 1919+21 — in which we can see evident decorrelation of the pulsar spectrum with increasing space separation between sources in the pulsar magnetosphere.

Measurements were made at 102.7 MHz using the Large-Aperture Synthesis Telescope (BSA) of the Lebedev Physics Institute at Pushchino (Russia) in April and June, 1994. We used a new $128\times1.25$ KHz multichannel receiver. Pulses were sampled every 5.12 ms in all 128 channels in a 300 ms window. We used the noise part of each recording for a baseline calibration and equalization of amplification in all channels.

For studing the decorrelation between pulsar spectra at separated longitudes we have calculated a mean cross-correlation functions between strong pulse ($S/N\geq5\sigma$) spectra taken at the longitude of the leading edge of the pulse profile and at all subsequent longitudes $l$. We will present the dynamic spectra of PSR 0834+06, 1133+16 and 1919+21 at separated longitudes. We can see obvious decorrelation of the spectra at remote longitudes. The strongest difference between spectra occur for PSR 1919+21. From the falling crosscorrelation coefficient $R(0)$ with increasing longitude separation $\Delta l$ we can obtain the space separation $\Delta r$ between sources.

78.03

**EGRET Gamma-Ray Observations of PSR B1706−44**

D.J. Thompson, D.L. Bertsch, C.E. Fichtel, R.C. Hartman, S.D. Hunter (NASA/GSFC), B.L. Dingus, J.A. Esposito, R. Mukherjee, J.R. Mattox (USRA/GSFC), G. Kanbach, H.A. Mayer-Hasselwander, M. Merck (MPE), C. von Montigny, P.V. Ramanamurthy (NAS/NRC), J.M. Fierro, Y.C. Lin, P.F. Michelson, P.L. Nolan (Stanford), D.A. Kniffen (Hampden-Sydney), E.J. Schneid (Grumman)

Observations with the Energetic Gamma Ray Experiment Telescope (EGRET) on the Compton Observatory have shown that radio pulsar PSR B1706−44 is a source of pulsed high-energy gamma radiation. With additional data, new details of the gamma radiation are found: The light curve appears to consist of two closely-space peaks. There is little, if any, unpulsed emission. The energy spectrum does not show significant evidence of a spectral break in the few GeV range, unlike the other pulsars seen by EGRET. These results, especially when combined with the ROSAT X-Ray (Becker *et al.* IAU Circ. No. 5554) and TeV gamma-ray observations (Kifune *et al.* IAU Circ. No. 5905) of this source, emphasize the diversity seen among the known gamma-ray pulsars.

78.04

**Soft X-Ray Emission from Isolated Pulsars: An Archival Study**

Nicole Lloyd (Cornell University), Patrick Slane (SAO)

Studying Soft X-ray emission from isolated pulsars is necessary to understand both the structure and dynamics of a neutron star. Surface emission associated with cooling of the hot interior allows one to probe the inner structure of the star, while emission associated with the pulsar spin-down power provides information on the magnetosphere.

Here we report initial results from an ongoing study of pulsar X-ray properties. We have derived upper limits to the surface temperatures of eight pulsars, and compared these temperatures with those predicted by standard cooling models. In addition, we derived X-ray luminosities (or upper limits) for each pulsar, assuming a Crab-like power law spectrum; these luminosities have been compared to those expected if the X-ray emission was entirely a result of the pulsar spin-down. For pulsars detected above the $3\sigma$ level, we performed spectral investigations to confront thermal cooling vs. spin-down scenarios for the origin of the emission. Some of the more interesting results from our investigation include a surface temperature for PSR 1822-09 which marginally constrains some standard neutron star cooling models, and evidence of spin-down origin for emission from PSR 0950+08 that is inconsistent with what is predicted by outer gap models. Additional work is being done on reported potential PSR/SNR associations for two pulsars, as well as on the correlation between pulsars' X-ray fluxes and their gamma-ray flux upper limits (as reported by EGRET).

78.05

**Towards VLBI Determination of Pulsar Parallaxes, Proper Motions, and Positions.**

N. Putnam (Brown University), R.M. Campbell (Harvard University), I.I. Shapiro (CfA)

Interleaved VLBI observations of a pulsar and one or more extragalactic phase-reference sources nearby on the sky provide a means to determine their differential positions with sub-milliarcsecond accuracy. Campbell *et al.* have begun a long-term program to determine the parallax distances, proper motions, and positions of about seven pulsars [see, *e.g.*, Campbell *et al.* 1993, in *Sub-arcsecond Radio Astronomy*, ed. R.J. Davis and R.S. Booth (Cambridge: Cambridge University Press), 420]. These results could be used to study the properties of the $\eta_e$ distribution in the solar neighborhood, the calibration of the dispersion-based galactic distance scale, and, when coupled with independent pulse time-of-arrival data, the tie between the extragalactic and dynamic reference frames. Here, we present results of work conducted under the 1994 SAO Summer Intern Program at the CfA within the broader context of the overall goals of the pulsar parallax project.

We acknowledge support from the NSF Research Experiences for Undergraduates Program (NP), NSF grant AST93-03527 (RMC,IIS), and NASA grant NGT-50663 (RMC).

78.06

**Evidence for Planets around PSR 0329+54**

T.V.Shabanova (Pushchino ASC,Russia)

The results of the analysis of available pulse arrival times of the pulsar PSR 0329+54 are presented. The total data set spans the period 25.7 years and consists of the Pushchino timing data between 1978 and 1994 and the JPL timing data between 1968 and 1983 (Downs & Reicley 1983, Ap.J.Suppl.Ser.,53,169, Downs & Krause-Polstorff 1986,Ap.J.Suppl.Ser.,62, 81). Analysis has shown, that timing residuals have a quasi-sinusoidal modulation with a period of 16.9 years. This periodicity may be interpreted as evidence for the existence of a planet-like body orbiting the pulsar PSR 0329+54 with the 16.9-yr orbital period. The planet has the minimum mass of about two masses of the Earth and moves in eccentric orbit (e=0.23) with the semimajor axis 7.3 AU. In 1979 Demianski and Proszynski in their paper 'Does PSR 0329+54 have companions?' reported the existence of sinusoidal modulation in the arrival times with a period of about 3 years (Nature,1979,282,383). In the present paper the existence of this 3-yr periodicity in the pulse arrival times is verified. It is manifested distinctively in the JPL data only after removing the main 16.9-yr periodicity.

78.07

**Gamma Ray Pulsars: Extended Polar Cap Cascades in Nearly Aligned Rotators**

J.K. Daugherty (UNCA), A.K. Harding (NASA/GSFC)

We have used a revised Monte Carlo simulation to estimate light curves and energy spectra for gamma ray pulsars, under the assumption that these objects have nearly aligned rotational and magnetic axes. Our simulation is based on a Polar Cap model in which the gamma rays are due to photon-pair cascades initiated by curvature radiation above the magnetic polar caps (PCs). In the nearly-aligned rotator scenario, even sources whose light curves have two distinct peaks (Crab, Vela, Geminga) are due to emission produced near the rim of a single PC. If the inclination $\alpha \sim \theta_{pc}$, the peak-to-peak phase separation can have the large values ($\sim 0.4-0.5$) observed from these sources. We can also attribute their nonzero interpeak emission to cascades above the PC interior. Our new simulations allow for a finite electron acceleration zone above the PC, which can extend to a height of several stellar radii. Our best fits to the observed light curves are obtained from models in which the accelerated electrons have a quasi-uniform surface density over the PC interior and a sharp density increase of $\sim 3$) near the rim. We suggest that such a density function may result from acceleration of secondary pairs created near the rim, where the open magnetic field lines have their maximum curvature and hence are most likely to produce pairs below the acceleration cutoff height. We note that the combined effects of moderately enlarged PC radii and extended acceleration zones provide a solution to a major difficulty with standard PC models, namely their small emission beams (and hence small detection probabilities). We show that our model results for Vela can reproduce key features of both the light curves and the phase-resolved energy spectra. Finally, we consider constraints imposed on nearly-aligned rotator models by observations at other wavelengths (radio, optical, X-ray).

78.08

**Broadening and Depolarization of Pulsar Average Profiles**

Mark M. McKinnon (NRAO)

Given the apparent correlation between the critical frequencies in the spectra of pulsar pulse width and fractional linear polarization, we develop a model of subpulse broadening and depolarization due to the birefringence of the plasma above pulsar polar caps. The broadening at low radio frequency is caused by the divergence of the individual beams of the two propagation modes, and the depolarization at high frequency results from the merger of their orthogonal polarizations. In addition to the critical frequency correlation, the model predicts rapid depolarization with frequency when the linear polarizations of the beams are comparable. The predictions are generally supported by multi-frequency observations of pulsar linear polarization and studies of individual pulse polarization. An interpretation of more recent observations in terms of the model suggests that they are consistent with an emission mechanism which is broad-band in frequency over a narrow range of emission altitudes. Old pulsars are found to depolarize faster than young ones, implying that the relative strength of the orthogonal polarization modes evolves with time.

78.09

**Refractive and Diffractive Scintillation of the Pulsar PSR B0329+54**

D. R. Stinebring (Oberlin College), M. D. Faison (U. Wisconsin), M. M. McKinnon (NRAO)

Refractive and diffractive scintillation are thought to be two related consequences of scattering in the interstellar medium. The predicted modulation of diffractive scintillation parameters by refractive effects has not been thoroughly tested, however. We report 24 days of scintillation observations of the radio pulsar PSR B0329+54 from September 1993 to June 1994 with a 26-m telescope operating at 610 MHz. Dynamic spectra were obtained on each day, from which the characteristic bandwidth and time scale of the diffractive scintillation pattern were determined. A relative flux value for the pulsar was also obtained on each day. The cross-covariance coefficient for

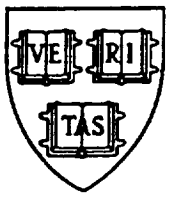


Harvard-Smithsonian
Center for Astrophysics

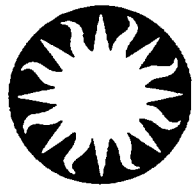

**Preprint Series**

No. 4156
(Received August 23, 1995)

# SOFT X-RAY EMISSION FROM SELECTED ISOLATED PULSARS

Patrick Slane and Nicole Lloyd
Harvard-Smithsonian Center for Astrophysics

To appear in
*The Astrophysical Journal (Letters)*
October 20, 1995

HARVARD COLLEGE OBSERVATORY SMITHSONIAN ASTROPHYSICAL OBSERVATORY
60 Garden Street, Cambridge, Massachusetts 02138

Center for Astrophysics
Preprint Series No. 4156

# SOFT X-RAY EMISSION FROM SELECTED ISOLATED PULSARS

Patrick Slane and Nicole Lloyd
Harvard-Smithsonian Center for Astrophysics

# Soft X-Ray Emission From Selected Isolated Pulsars

Patrick Slane and Nicole Lloyd [1]
Harvard-Smithsonian Center for Astrophysics
60 Garden Street
Cambridge, MA 02138
E-mail: slane@cfa.harvard.edu, lloyd@cfa.harvard.edu

## ABSTRACT

The soft X-ray emission from isolated neutron stars (NSs) may originate from a number of processes, each of which probes a unique characteristic of the interior or magnetospheric structure. In order to characterize this emission in the context of current models, we have begun an archival investigation of such emission using data from the ROSAT Observatory. Here we report on analysis for seven pulsars based upon data taken with the ROSAT Position Sensitive Proportional Counter (PSPC). For each pulsar, we derive upper limits for the NS surface temperature as well as luminosity values or upper limits associated with a Crab-like power law interpretation. Several of the pulsars were detected, and for these we have investigated scenarios for emission associated with the cooling of the hot NS interior as well as with the pulsar spin down. The emission from PSR 2334+61 and PSR 0114+58 appears consistent with a spin-down origin, although we cannot rule out emission associated with cooling of the NS interior. For PSR 1822–09, we find that the surface temperature upper limit implied by the non-detection falls below the predictions of several cooling models, potentially providing constraints on interpretations of the interior equation of state. Emission from the vicinity of PSR 1642–03 may be produced by an extended synchrotron nebula associated with the pulsar, but such models appear problematic. Alternatively, the observed flux may be produced by a background object in the field of the pulsar position.

*Subject headings:* Pulsars: general — radiation mechanisms: non-thermal — radiation mechanisms: thermal — X-rays: stars

---

Accepted for Publication in *The Astrophysical Journal Letters*

---

[1]Present address: Astronomy Dept., Cornell University, Ithaca, NY 14853

## 1. INTRODUCTION

X-ray emission from isolated pulsars is typically associated with either cooling of the neutron star interior, magnetospheric processes which derive energy from the pulsar spin-down, or a combination of these. Accretion from the interstellar medium may also produce measurable flux in regions where the accretion rate is particularly favorable. The X-ray flux associated with these mechanisms is typically soft, and the sources themselves are generally relatively faint. Imaging X-ray telescopes with large effective area in the 0.1–1.5 keV band are optimum for the study of these objects as results from the *Einstein* and ROSAT missions have shown. The reader is referred to recent reviews by Ögelman (1995) and Finley (1995) for summaries of the current status of such X-ray studies. Here we study emission from a set of isolated pulsars using data from the ROSAT public data archive in order to investigate specific emission scenarios, and to compare results with those obtained for other pulsars.

The pulsars for which analysis is presented are listed in Tables 1 and 2 along with information regarding the PSPC observations. These pulsars were selected on the basis of: 1)likelihood of detection based upon pulsar age, spin-down rate, distance, and dispersion measure; and 2)adequate exposure time to provide interesting limits on the NS surface temperature. Brief results for PSR 2334+61 have been reported by Becker *et al.* (1994). Results for PSRs 0740–28, 1822–09, and 1916+14 have also recently appeared elsewhere (Alpar *et al.* 1995). Our analysis approach differs in several ways from those used above, and we present our results here to provide improved limits on some measurements and to place all the measurements in a common context of alternative emission scenarios.

We begin with a description of the data reduction and analysis procedures. We then summarize the results for each pulsar and, where appropriate, discuss the results in the context of models for X-ray emission from isolated pulsars. We conclude with a comparison of results to those for other pulsars and summarize the main conclusions of our analysis.

## 2. Data Selection and Analysis

The PSPC on-axis point response function can be approximated by the sum of 3 components (Hasinger *et al.* 1992) which, for the soft emission characteristic of pulsars, is dominated by the Gaussian term associated with the finite spatial resolution of the PSPC. For photons of energy $\sim 0.5$ keV, the width of the Gaussian is $\sigma \sim 0.2$ arcmin. For the observations under investigation, the background level is approximately

$5 \times 10^{-4}$ counts arcmin$^{-2}$ s$^{-1}$ and the integration times are $\sim 5 - 10$ ks; the count rate for a source at the threshold of detectability is thus $\sim 10^{-3}$ counts s$^{-1}$. For these parameters, the signal-to-noise ratio is maximized with a detect cell of radius $\sim 0.5$ arcmin. We have thus used a circle of radius 0.5 arcmin, centered at the radio position (Taylor *et al.* 1993) of the pulsar, to extract counts for each dataset. The total number of counts was then obtained by scaling by the appropriate factor ($\sim 1.1$) to account for the encircled fraction within the detect cell. The background level was determined by extracting counts from an annulus extending from 3-13 arcmin around the source position; each field was investigated for the presence of other sources in the background region and any such sources were removed. For detect cells containing fewer than 20 counts, 95% confidence interval count rates or upper limits were determined using a Bayesian statistical approach (Kraft *et al.* 1991).

To determine the surface temperature upper limits, we assumed a NS radius of 10 km, and distance values were obtained from (Taylor *et al.* 1993). Where available, we used HI absorption measurements to determine the value of $N_H$, assuming a neutral hydrogen spin temperature $T_s = 100$ K. When unavailable, $N_H$ was determined by scaling that for the Crab pulsar by the ratio of dispersion measures. Using this information to determine the normalization and absorption, we then calculated the blackbody temperature required to produce the observed count rate when the spectrum is folded through the PSPC spectral response matrix. For cases in which the implied spectrum was extremely soft (PSRs 1822–09 and 0031–07) an additional correction of $\sim 20\%$ was added to the factor of 1.1 discussed above to account for the fact that the PSPC encircled fraction is broader at lower energies. These values, corrected for gravitational redshift effects at the site of emission, are listed in Table 2 and plotted in Figure 1. Also plotted are theoretical cooling curves for a number of models based upon different assumptions for interior structure of the NS. We note that the bulk of the derived values are consistent with standard cooling scenarios which do not require the presence of exotic matter in the NS core, nor operation of the direct URCA process. As discussed below, for PSR 1822–09 the derived value appears inconsistent with the models of Nomoto and Tsuruta (1987). The derived temperature limit does depend upon several uncertain factors such as the NS radius and distance, and the value of $N_H$. Further observations of this pulsar, at higher sensitivity, are particularly important in this regard.

For the case of magnetospheric emission, where the X-ray luminosity is derived from the spin-down power, we assumed a Crab-like power law spectrum with energy index $\alpha_E = 1$ to derive the luminosity which corresponds to the observed count rate or upper limit. Distance and $N_H$ values were determined as described above. The resulting luminosity values are presented in Table 2 and plotted in Figure 2, which is discussed further in Section 4.

Since, for the detected pulsars, the number of counts is very small, spectral fitting to derive the emission characteristics is not practical. Similarly, the sparse statistics do not permit meaningful timing analysis.

## 3. Results

Because the exposure time and relative fluxes for the various pulsars differ considerably, the level of analysis varies from source to source. Here we describe the results of our analysis for each of the sources investigated.

*PSR 1642–03:* *Einstein* IPC observations of this pulsar reveal weak X-ray emission located $\sim 50$ arcsec from the radio position (Helfand 1983). Lack of detection with the *Einstein* HRI led to the suggestion that the emission is extended on scales of $\sim 60 - 90$ arcsec, thus appearing pointlike in the IPC but yielding a surface brightness below detectability in the HRI exposure. These results led Cheng (1983) to propose that PSR 1642–03 (along with several other pulsars) may support a synchrotron nebula which is confined by the ram pressure generated as the pulsar wind is driven into the ISM.

Emission from the vicinity of PSR 1642–03 is also detected in the PSPC (Slane 1994a), with a count rate $R = (8.7 \pm 3.2) \times 10^{-3}$ s$^{-1}$. Unfortunately, the proposed 40 ks observation was truncated to only 3.1 ks. The resulting spectrum is thus too sparse to perform detailed spectral investigations. The parameters derived for surface cooling and power law scenarios are given in Table 2 where we have used $N_H = 1.0 \times 10^{21}$ cm$^{-2}$ as derived from HI absorption measurements (Sancisi and Klomp 1972). The temperature limit of $T_0 < 10^{6.1}$ K falls far above any cooling curves for a pulsar of this age. If the emission is from the pulsar, it is clearly not generated from cooling of the interior. On the other hand, the luminosity suggested by a Crab-like spectrum is considerably higher than expected based upon the spin-down power (Figure 2). If associated with the pulsar, this suggests either a unique geometry or a different emission mechanism than that observed for other pulsars.

The emission observed in the PSPC is also offset from the pulsar position. With a separation of $\sim 1$ arcmin, the offset is unlikely to be associated with poor aspect or the finite detector resolution, particularly since the same results were observed with the IPC. Rather, the emission is either associated with a background source or with extended emission associated with the pulsar. We have considered two scenarios in the latter category. For emission from a standard synchrotron nebula with a power law electron energy distribution confined by an ambient magnetic field, assuming equipartition between the total electron and magnetic field energies (Ginzburg and Syrovatskii 1965), a Crab-like spectrum requires

a relatively small magnetic field ($\sim 10^{-5}$ G) as well as a modest energy content for the X-ray emitting electrons ($\sim 8 \times 10^{43}$ erg). However, assuming continuous ejection of the electron spectrum over the life of the pulsar leads to a predicted radio flux of nearly 150 mJy, much larger than that associated with PSR 1642-03. Such a synchrotron scenario is thus implausible in the absence of some relatively recent increase in the electron flux.

Alternatively, the emission may be associated with a synchrotron nebula which is confined by the ram pressure of the electron wind driven by the pulsar motion through the ISM (Cheng 1983). In this model, a reverse shock forms in the direction of the pulsar motion. Synchrotron emission is then produced in a region extending beyond the shock radius, which depends upon the pulsar velocity as well as the ambient ISM density. The proper motion for PSR 1642-03 yields a projected velocity $v_\perp \approx 6.6 \times 10^7$ cm s$^{-1}$, in a direction consistent with the offset between the radio pulsar position and the observed X-ray emission, as the model would predict. The flux is a function of the magnetization parameter, $\sigma$, equal to the ratio of the Poynting flux to the particle energy flux. We have calculated the model predictions for the X-ray flux as a function of shock radius for various values of $\sigma$. We have assumed $\sigma_s$, the value at the shock, is $\sim 1$; smaller values correspond to a higher efficiency for converting the upstream energy flux to randomized particle energy, and the resulting spatially extended emission is stronger than that observed. We note that the EGRET upper limit for this pulsar (Thompson *et al.* 1994) requires $\alpha_E > 0.6$ assuming the spectral index extends to $\gamma$-ray energies.

For the range of $\alpha_E$ investigated ($0.6 < \alpha_E < 2.0$), the models can successfully reproduce the observed X-ray flux. However, in each case the predicted radio flux is much too large. The volume of the emitting region may correspond to a region smaller than the full 1 arcmin offset from the pulsar position, which would reduce the predicted flux by a proportional factor. However, there is still difficulty in extending the flux to the radio range, particularly since the radio spectral index is $\alpha_E \sim 2$.

Spectral observations of higher sensitivity are warranted to further investigate the emission. Extended synchrotron emission from PSR 1642–03 cannot be ruled out, but the models considered have difficulty reproducing the overall emission characteristics of the pulsar. It appears distinctly possible that the observed flux is associated with a source other than the pulsar. Inspection of the Digitized Sky Survey plates reveals a faint optical source coincident with the observed X-ray emission, which we suggest as a possible counterpart.

*PSR 0114+58:* This pulsar was detected with a 95% confidence interval for the count rate at $(1.7 - 5.0) \times 10^{-3}$ s$^{-1}$; a non-detection is rejected at greater than the 99.99% confidence level. As indicated in Figure 1, the associated temperature upper limit for blackbody

emission from the entire NS surface does not present any constraints on current cooling models. The fact that the characteristic temperature falls above all cooling curves suggests that the bulk of the emission is derived from the pulsar spin-down. This is consistent with the $L_x$ vs. $\dot{E}$ relationship indicated in Figure 2, which is similar to that for other pulsars. Assuming a Crab-like spectrum which extends to $\gamma$-ray energies, the X-ray data predicts $F(E > 100\mathrm{MeV}) = 1.9 \times 10^{-10}$ photons cm$^{-2}$ s$^{-1}$, consistent with the reported EGRET upper limit of $2.3 \times 10^{-7}$ photons cm$^{-2}$ s$^{-1}$ (Thompson *et al.* 1994).

*PSR 1822–09:* Although undetected in the 5.2 ks PSPC exposure, the upper limit to the count rate for this pulsar provides an interesting constraint on models for cooling of the NS interior. PSR 1822–09 is of moderate age (characteristic age $\tau = 10^{5.4}$ y) and relatively nearby ($D = 1.03$ kpc). Lack of detection implies a surface temperature $T_s < 10^{5.85}$ K (corrected for gravitational redshift at the NS surface) assuming blackbody emission from the entire surface and using $N_H = 9 \times 10^{20}$ cm$^{-2}$ derived from 21-cm measurements (Gómez-Gonzàlez and Guélin 1974). As illustrated in Figure 1, this upper limit is lower than the temperatures predicted by Nomoto and Tsuruta (1987). In fact, the Nomoto and Tsuruta models shown actually illustrate $T_\infty$, the surface temperature uncorrected for gravitational redshift, which is lower by a factor of $\sim 1.1 - 1.4$ than the corrected surface temperature. Including corrections for the NS radii for the equations of state used in these models, we find $T_\infty = (5.0 - 5.8) \times 10^5$ K, considerably below the model curves. In addition, we have neglected any contribution from a NS atmosphere. The presence of an atmosphere would modify the blackbody spectrum, producing a harder tail and resulting in an effective temperature which is higher than the actual surface temperature; omission of the effects of the atmosphere thus tend to overestimate the temperature, which implies that the derived upper limit is solid (Romani 1987, Miller 1992, Shibanov *et al.* 1992). The derived upper limit to the blackbody luminosity $L_{\mathrm{BB}} < 1.8 \times 10^{32}$ erg s$^{-1}$ is consistent with that calculated by Alpar *et al.* (1995). We note, however, that uncertainties in $N_H$ lead to uncertainties in the derived temperature upper limit. Scaling the dispersion measure for PSR 1822–09 to that of the Crab pulsar suggests $N_H = 1 \times 10^{21}$ cm$^{-2}$, in good agreement with the 21-cm value. However, both methods require assumptions which may be inaccurate for this particular region. A lower $N_H$ value reduces the temperature upper limit. However, a value twice as large as that used would lead to $T_s < 10^{5.95}$ K, which does not conflict with the cooling models. Further observations of this pulsar are thus of great interest.

*PSR 2334+61:* This pulsar is detected with a PSPC count rate of $(0.5–2.6) \times 10^{-3}$ counts s$^{-1}$, in good agreement with the value reported by Becker *et al.* (1994). The derived blackbody and power-law luminosities listed in Table 2 are both in good agreement with the models and empirical results for other pulsars. With limited statistics, spectral fits to the PSPC

data were not possible. We have derived hardness ratios from the data and compared these with models for blackbody emission from the stellar surface as well as for Crab-like power law emission (see Slane 1994b). However, the hardness ratio error bars are sufficiently large to prevent ruling out either interpretation. As with PSR 0114+58, extension of a Crab-like spectrum to higher energies predicts a flux well below current upper limits from EGRET (Thompson *et al.* 1994).

An association between PSR 2334+61 and the supernova remnant (SNR) G114.3+0.3 has been suggested by Kulkarni *et al.* (1993) based upon relative positions as well as estimated distances and ages for the two objects. We do not observe emission from the SNR in the PSPC image. The expected size, based upon the radio image, is $R = 25$ arcmin; thus the image is expected to encompass the bulk of the inner region of the PSPC and could be hard to detect if it is faint. If we assume a Sedov solution for the SNR, using the pulsar age and distance, the inferred shock temperature is $\sim 5 \times 10^5$ K. This is sufficiently cool for the remnant to have entered the radiative phase, in which case we expect the X-ray luminosity to be somewhat low. Deeper X-ray observations of the SNR are required to more fully assess the remnant properties and to place further constraints on the suggested association between these objects.

*PSRs 0031–07, 0740–28, and 1916+14:* These pulsars are all undetected in the PSPC exposures. The characteristics implied by the flux upper limits are summarized in Table 2. We note that count rate limits for PSR 0740–28 and PSR 1916+14 have been reported by Alpar *et al.* 1995. However, the upper limits derived here are lower in each case. This is explained in part by the fact that the previous authors extracted counts from a circle of radius 80 arcsec, thus incorporating considerably higher background than we have allowed. In addition, Alpar *et al.* considered only $\sim 1.8$ ks of data for PSR 0740–28 where we have used the full 4.5 ks exposure. Finally, we have used HI absorption measurements to obtain $N_H$ values for PSR 0740–28 (Gómez-Gonzàlez and Guélin 1974), and PSR 0031–07 (Sancisi and Klomp 1972). The NS surface temperature upper limits implied by the observations are consistent with standard models for interior cooling.

## 4. Conclusions

We have analyzed X-ray data from 7 isolated pulsars using archival ROSAT PSPC data. Two of the pulsars, PSRs 0114+58 and 2334+61, are detected. Emission is also observed in the vicinity of PSR 1642–03, but the overall energy considerations may rule out an assoication with the pulsar and the X-ray emission; a spin-down scenario would require extremely high efficiency for conversion of rotational energy to X-ray luminosity

while extended synchrotron nebulae models can reproduce the X-ray flux, but then grossly overpredict the radio flux. Using a Crab-like power law spectrum, we have derived X-ray luminosities for these pulsars and compared these with the available spin-down power. The results are plotted in Figure 2 where we have also plotted such results for other detected pulsars (Ögelman 1995). The values for the pulsars detected here are consistent with an empirical $L_x - \dot{E}$ relationship derived by Seward and Wang (1988) and Ögelman (1995), as indicated in the Figure.

The uncertainty in the flux for PSRs 0114+58 is somewhat large due to the fact that the pulsar is rather faint; while clearly detected in the optimized detect cell chosen for this analysis, deeper observations are clearly of interest to refine the luminosity calculations and to search for pulsations. Similarly, additional observations of PSR 2334+61 are of interest in order to search for pulsations as well as to obtain more detailed information regarding the X-ray emission from G114.3+0.3.

While we have not detected emission from PSR 1822–09, the count rate upper limit provided by the PSPC observation places interesting constraints on one set of cooling models. Deeper observations of this pulsar will either yield a detection or will provide even more powerful constraints on such models.

The authors would like to thank F. Primini for helpful discussions on source detection and F. Rick Harnden for useful comments on the text. This work was supported by the National Aeronautics and Space Administration through grant NAG5-2329, and contract NAS8-39073, and by the National Science Foundation through the SAO Summer Intern Program.

Table 1

Pulsar Parameters

| Name | $P$ (s) | $\dot{P}$ ($\times 10^{-14}$ s s$^{-1}$) | DM (pc cm$^{-3}$) | $D$ (kpc) | $\log \tau$ (yr) | $\log \dot{E}$ (erg s$^{-1}$) |
|---|---|---|---|---|---|---|
| 0031–07 | 0.943 | 0.041 | 10.89 | 0.68 | 7.56 | 31.28 |
| 0114+58 | 0.101 | 0.584 | 49.45 | 2.14 | 5.44 | 35.34 |
| 0740–28 | 0.167 | 1.681 | 73.77 | 1.89 | 5.20 | 35.16 |
| 1642–03 | 0.388 | 0.178 | 35.66 | 2.90 | 6.54 | 33.08 |
| 1822–09 | 0.769 | 5.236 | 19.46 | 1.01 | 5.37 | 33.66 |
| 1916+14 | 1.181 | 21.140 | 30.00 | 1.55 | 4.95 | 33.70 |
| 2334+61 | 0.495 | 19.191 | 58.38 | 2.47 | 4.61 | 34.80 |

Table 2

X-Ray Characteristics

| Name | Exposure (ks) | $R_{\rm PSPC}$ ($\times 10^{-3}$s$^{-1}$) | $\log N_H$ (cm$^{-2}$) | $\log T_{\rm up}$ (K) | $L_{bol}$(BB) (erg s$^{-1}$) | $L_x$(PL)[c] (erg s$^{-1}$) |
|---|---|---|---|---|---|---|
| 0031–07 | 7.9 | $< 1.2$ | 20.60(a) | 5.64 | $< 2.7 \times 10^{31}$ | $< 1.5 \times 10^{30}$ |
| 0114+58 | 4.7 | 1.7–5.0 | 21.41(b) | 6.04 | $1.1 - 1.7 \times 10^{33}$ | $4.7 - 14 \times 10^{31}$ |
| 0740–28 | 4.5 | $< 2.0$ | 21.26(a) | 6.01 | $< 8.0 \times 10^{32}$ | $< 3.7 \times 10^{31}$ |
| 1642–03 | 3.2 | 5.5–11.9 | 21.0(a) | 6.12 | $1.3 - 2.1 \times 10^{33}$ | $1.8 - 3.9 \times 10^{32}$ |
| 1822–09 | 5.2 | $< 1.8$ | 20.95(a) | 5.86 | $< 2.0 \times 10^{32}$ | $< 6.9 \times 10^{30}$ |
| 1916+14 | 2.0 | $< 3.7$ | 21.20(b) | 6.01 | $< 8.0 \times 10^{32}$ | $< 4.1 \times 10^{31}$ |
| 2334+61 | 8.7 | 0.5–2.6 | 21.49(b) | 6.06 | $0.8 - 1.6 \times 10^{33}$ | $2.1 - 11.0 \times 10^{31}$ |

(a) $N_H$ derived by 21-cm measurements (see text)

(b) $N_H$ scaled to the Crab by dispersion measures

(c) luminosity in 0.1–2.4 keV band

## REFERENCES

Alpar, M. A., Guseinov, O. H., Kiziloğlu, Ü., and Ögelman, H. 1995, A&A 297,470.

Becker, W., Trümper, J., & Ögelman, H. 1994, IAU Circular #5805.

Cheng, A. F. 1983, ApJ, 275, 790.

Finley, J. P. 1995, to appear in Proceedings of the ROSAT Science Symposium.

Ginzburg, V. L., and Syrovatskii, S. I. 1965, Ann. Rev. Astron. & Astrophys., 3, 297.

Gómez-Gonzàlez, J., and Guélin, M. 1974, A&A, 32, 441.

Hasinger, G., Turner, T. J., George, I. M., and Goese, G. 1992, *Legacy* No. 2, 77.

Helfand, D. J. 1983, in *Supernova Remnants and Their X-Ray Emission*, eds. J. Danzinger & P. Gorenstein (Dordrecht: Reel), p. 335.

Kraft, R. P., Burrows, D. N., and Nousek, J. A. 1991, ApJ, 374, 344.

Kulkarni, S. R., Predehl, P., Hasinger, G., and Aschenbach, B. 1993, Nature, 362, 135.

Miller, M. C. 1992, MNRAS, 255, 129

Nomoto, K., & Tsuruta, S. 1987, ApJ, 305, L19

Ögelman, H. 1995, in *Lives of Neutron Stars*, eds. M.A. Alpar, U. Kiziloglu, & J. van Paradijs, NATO ASI Ser. C: Vol. 450, p. 101.

Page, D., & Baron, E., 1990, ApJ 354, L17

Romani, R. W. 1987, ApJ, 313, 718.

Sancisi, R. and Klomp, M. 1972, A&A, 18, 329.

Seward, F. D., & Wang, Z-R 1988, ApJ, 332, 199

Shibazaki, N., & Lamb, F. K., ApJ, 346, 808, 1989

Shibanov, Y. A. *et al.* 1992, A&A, 266, 313

Slane, P. 1994a, in *New Horizon of X-Ray Astronomy – First Results From ASCA*, eds. F. Makino and T. Ohashi (Universal Academy Press), p. 423.

Slane, P. 1994b, ApJ, 437, 458.

Taylor, J. H., Manchester, R. N., & Lyne, A. G. 1993, ApJ Supp., 88, 529

Thompson, D. J. *et al.* 1994, ApJ, 436, 229.

---

This preprint was prepared with the AAS LaTeX macros v3.0.

## FIGURE CAPTIONS

**Figure 1:** Models for cooling of neutron star interior. References to models are given in text. Shibazaki and Lamb Model 1 is for standard cooling with no reheating (lower) and reheating due to frictional coupling between crust and superfluid core; Model 2 includes effects of pion condensates in core. Page and Baron models are for no superfluid, no exotic matter (upper) and superfluid with kaon condensates (lower). Nomoto and Tsuruta models contain no exotic core matter, and: superfluid (lower), and no superfluid (upper) for soft equation of state; no superfluid (middle) with stiff equation of state. The temperature upper limit derived for PSR 1822–09 appears to rule out several of the standard cooling models. See text for discussion.

**Figure 2:** X-ray luminosity vs. spin-down power for known X-ray emitting isolated pulsars (after Seward and Wang 1988); luminosity values are from Ögelman (1994), Slane (1994b) and this paper. Pulsars from this paper are indicated by triangles (except for PSR 1643–03 which is indicated by a star to indicate an unlikely association). Closed triangles correspond to detected sources while open triangles are upper limits for undetected sources.

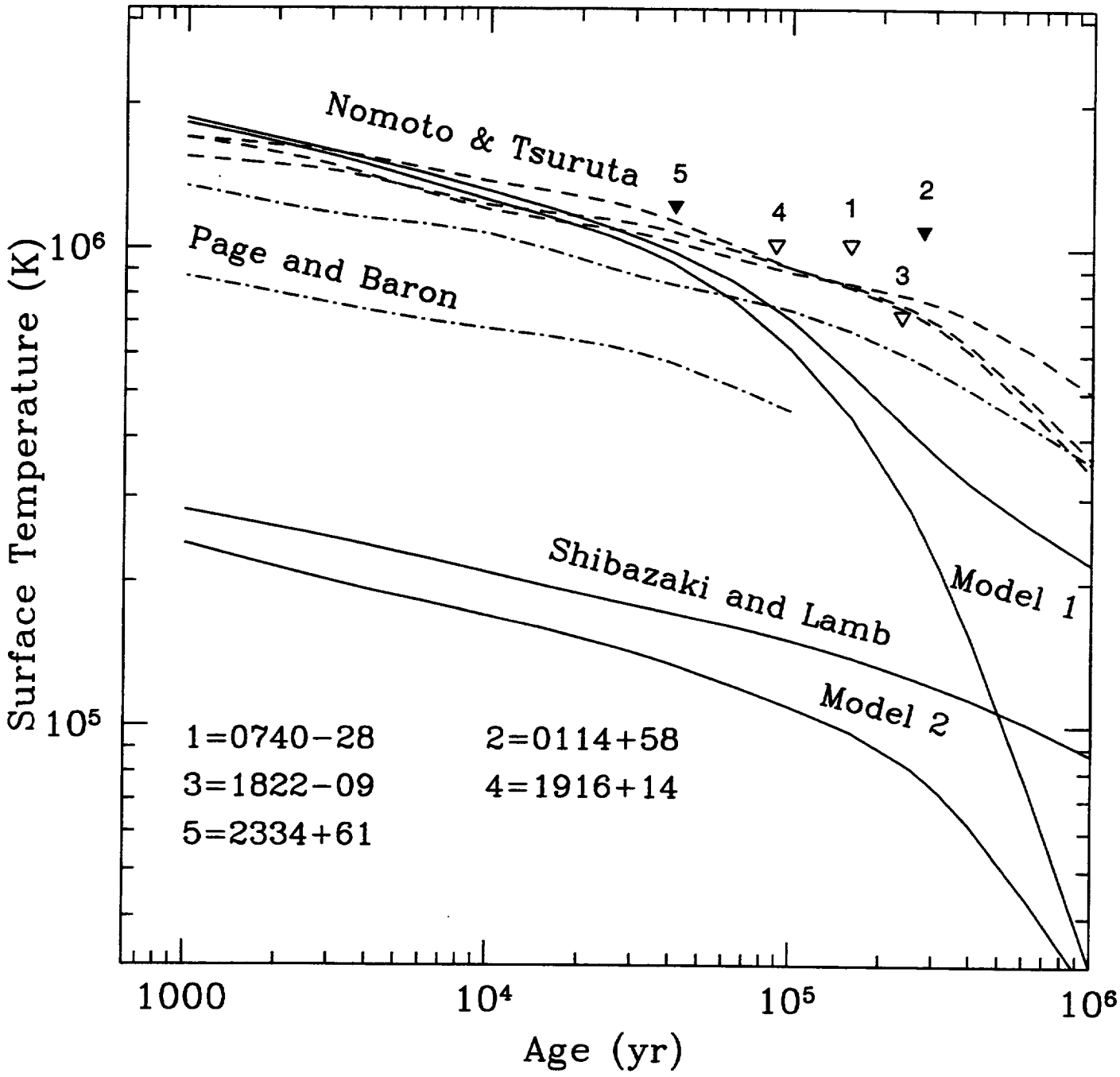
Nomoto & Tsuruta
Page and Baron
Shibazaki and Lamb
Model 1
Model 2
1=0740−28
2=0114+58
3=1822−09
4=1916+14
5=2334+61
Surface Temperature (K)
$10^6$
$10^5$
1000
$10^4$
$10^5$
$10^6$
Age (yr)

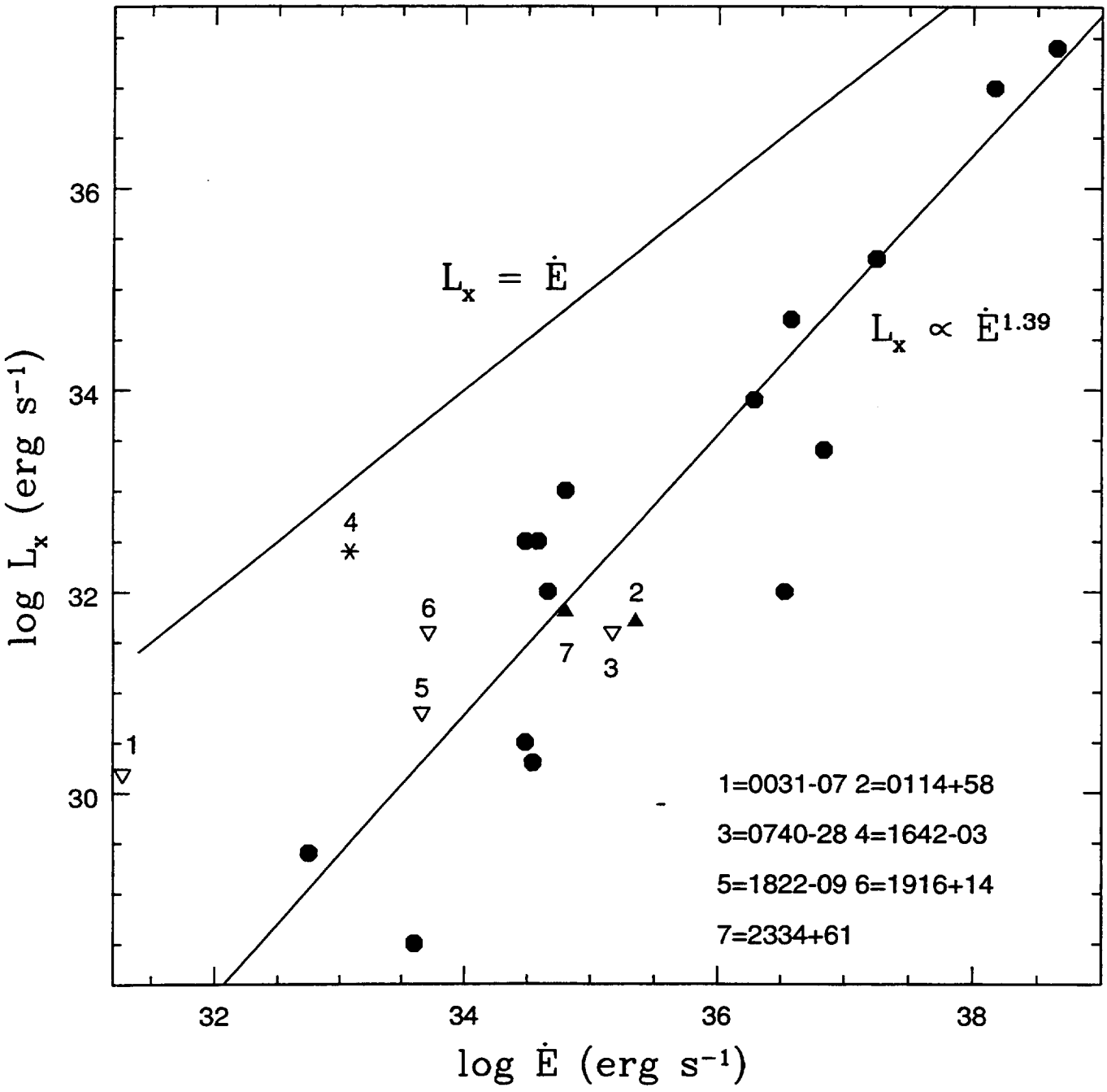
$L_x = \dot{E}$
$L_x \propto \dot{E}^{1.39}$
1=0031-07 2=0114+58
3=0740-28 4=1642-03
5=1822-09 6=1916+14
7=2334+61
log $L_x$ (erg $s^{-1}$)
log $\dot{E}$ (erg $s^{-1}$)
30
32
34
36
38


# Harvard-Smithsonian Center for Astrophysics

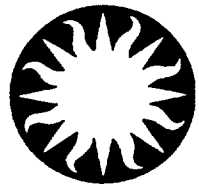

**Preprint Series**

No. 3898
(Received June 24, 1994)

## X-RAY EMISSION FROM PSR 0355+54

Patrick Slane
Harvard-Smithsonian Center for Astrophysics

To appear in
*The Astrophysical Journal*
December 10, 1994

Center for Astrophysics
Preprint Series No. 3898

# X-RAY EMISSION FROM PSR 0355+54

Patrick Slane
Harvard-Smithsonian Center for Astrophysics

# X-Ray Emission From PSR 0355+54

Patrick Slane
Harvard-Smithsonian Center for Astrophysics
60 Garden Street
Cambridge, MA 02138
E-mail: slane@cfa.harvard.edu

## ABSTRACT

We have obtained a 20 ks observation of PSR 0355+54 using the ROSAT PSPC. The pulsar is detected with a count rate of $4.2(\pm 1.3) \times 10^{-3}$ s$^{-1}$ above the background. While the $\sim$ 70 source counts are insufficient for spectral fitting, we have derived source parameters for specific cases of power law as well as blackbody spectra. For a Crab-like spectrum (photon index $\alpha = 2$) we find $L_x(0.1 - 2.4 \text{ keV}) = 1.0 \times 10^{32}$ erg s$^{-1}$, somewhat higher than upper limits reported from *Einstein* observations but consistent with typical $L_x$ vs $\dot{E}$ values for other pulsars. For blackbody emission, we derive a temperature upper limit of $\sim 9.5 \times 10^5$ K for emission from the entire neutron star surface, which is consistent with standard models for cooling of the neutron star interior given a characteristic age $10^{5.75}$ yr. No evidence is present for modulation at the 156 ms pulsar period, setting a weak upper limit of $\sim$ 75% for the pulsed fraction of the X-ray signal.

*Subject headings:* pulsars: individual (PSR 0355+54 ) — radiation mechanisms: non-thermal — X-rays: stars

## 1. INTRODUCTION

X-ray emission from isolated pulsars can originate from a number of distinct mechanisms. These can be categorized in terms of the energy source: cooling of the hot stellar interior; energy derived from the pulsar spin-down; or gravitational energy released upon accretion of material from the interstellar medium (ISM). The exact mechanism by which energy is produced in the X-ray band differs with each such scenario, and may actually consist of several modes and/or production sites. Cooling, for example, manifests itself as blackbody emission from the entire surface of the neutron star (NS). However, the spectrum may be modified by the presence of a thin atmosphere, and the details of the atmospheric effects depend upon the surface magnetic field strength. Further, thermal conductivity gradients across the surface, produced by the star's magnetic field, may result in a nonuniform surface temperature. Spin-down energy, associated with acceleration of charged particles in the pulsar magnetosphere, may take the form of thermal emission from the heated polar caps, synchrotron radiation produced near the pulsar light cylinder, or a synchrotron nebula supported by the ambient medium and magnetic field. Accretion luminosity may be thermal or nonthermal depending upon the exact mechanism by which the matter reaches the NS surface. Studies of the X-ray emission from isolated pulsars may thus provide information about the interior stellar structure, the surface characteristics of the NS, and the geometry and dynamics of the pulsar magnetosphere and its surroundings. The reader is referred to recent reviews by Ögelman (1994) and Finley (1994) for summaries of the current status of such X-ray studies. Here we study emission from PSR 0355+54 to investigate specific emission scenarios, and to compare results with those obtained for other pulsars.

PSR 0355+54 is a moderate age isolated pulsar (characteristic age $P/2\dot{P} = 10^{5.75}$ yr) with a fairly short period (156 ms). Radio studies show the pulsar to have relatively low timing noise, though occasional glitches have been observed including a massive glitch ($\Delta P/P = -4.4 \times 10^{-6}$) in 1986 (Lyne 1987) which was accompanied by a large change in spin-down rate. The post-glitch relaxation was studied by Alpar *et al.* (1988) in the context of a vortex creep model which describes the dynamical coupling of superfluid regions in the NS interior to the crust rotation. The primary properties as determined by radio observations (Taylor *et al.* 1993) are summarized in Table 1 where we have also listed properties for the similar pulsar PSR 1055–52.

Using the spin-down energy loss rate, $\dot{E}$, as an indicator, PSR 0355+54 is a good candidate for observable X-ray emission; only 10 of the 119 radio pulsars with distances, $D$, closer than PSR 0355+54 have larger values of $\dot{E}/D^2$, and 8 of these are known

X-ray emitters. X-ray observations of PSR 0355+54 were carried out with the *Einstein* Observatory, in a 19 ks pointing with the Imaging Proportional Counter (IPC), but the results were inconclusive. Weak emission from a position $\sim$ 1.7 arcmin from the radio position was detected, and Helfand (1983) suggested this could be evidence for extended emission from a synchrotron nebula associated with the pulsar. Seward and Wang (1988) considered the association tentative, reporting only an upper limit of $L_x < 4.8 \times 10^{31}$ ergs s$^{-1}$.

The study of this pulsar is particularly interesting because its properties are very similar to those of PSR 1055–52 (see Table 1), a known X-ray source (Cheng and Helfand 1983, Brinkmann and Ögelman 1987, Ögelman and Finley 1993) which has recently been detected as a $\gamma$-ray source as well (Fierro *et al.* 1993). The properties of PSR 0355+54 suggest a Vela-like pulsar very near the outer-gap death line for sustained $\gamma$-ray production (Chen and Ruderman 1993 – see Section 4), although it must be noted that this interpretation is somewhat dependent upon the inclination of the magnetic field relative to the pulsar spin axis; PSR 1055–52 has a radio pulse-interpulse separation of $\sim$ 180° (McCulloch *et al.* 1978), suggesting a large inclination angle, while the PSR 0355+54 radio profile shows a single peak (Morris *et al.* 1981) suggestive of a smaller inclination angle.

## 2. OBSERVATIONS

PSR 0355+54 was observed for 19,144 s, beginning on 13 March 1993, using the ROSAT Position Sensitive Proportional Counter (PSPC). The PSPC (Pfeffermann *et al.* 1986) provides coarse energy resolution [$\Delta E/E = 0.43(E/0.93)^{-0.5}$ (FWHM)] over the bandpass 0.1–2.4 keV along with position resolution of $\sim$ 25 arcsec (FWHM). Event times are recorded with relative accuracies of $\sim$ 100 $\mu$s, but absolute time uncertainties as large as 2 ms may occur over long periods (several days) due to clock drifts or resets. The PSR 0355+54 observation was carried out in 16 small segments spread over a $\sim$ 3 d period. After cleaning the data by removing any time intervals at the ends of these segments which showed evidence of increases in count rate due to bright Earth effects, 16,644 s of good data remained. A faint X-ray source was detected at a nominal position RA(J2000) = 03h 58m 53.2s, Dec(J2000) = +54° 13′ 00.6″, in good agreement with the pulsar position RA(J2000) = 03h 58m 53.7s, Dec(J2000) = +54° 13′ 13.58″ (Taylor *et al.* 1993 – see Figure 1). The position discrepancy (13.7 arcsec) is within the expected deviations based upon the spatial response of the detector and the limited number of counts in the image. The pulsar count rate was determined by extracting counts inside a circle of radius 2.5 arcmin centered on the source, using an annular region extending from 2.5 - 8.3 arcmin for background

determination. We find $N = 70.6 \pm 21.7$ source counts, corresponding to a count rate of $R_{\rm PSPC} = 4.2(\pm 1.3) \times 10^{-3}$ s$^{-1}$. Data were restricted to PI bins 11–235 (PROS channels 3–33), corresponding to an energy band $\sim 0.1 - 2.4$ keV.

To search for evidence of extended emission we have smoothed the x-ray image with a 32 arcsec Gaussian profile, and subtracted an identically selected and smoothed image of the calibration point source 3C273 normalized to the same number of (background-subtracted) counts. The resulting profile indicates faint emission concentrated $\sim 1.6$ arcmin from the pulsar, at a position angle approximately 72° north of east. This is consistent with the size of the offset described by Seward and Wang (1988) although the relative brightness of this region of enhancement is more than a factor of 5 smaller than that corresponding to the pulsar. The measured proper motion for PSR 0355+54 is $\mu_\alpha = 5 \pm 4$ mas yr$^{-1}$, $\mu_\delta = 6 \pm 3$ mas yr$^{-1}$ (Lyne *et al.* 1982). The sky projection of this motion corresponds, within uncertainties, to the direction to the enhanced emission. This may indicate that the emission, which appears ahead of the pulsar motion, is the result of synchrotron radiation from a wind-driven nebula supported by the ram pressure created by the proper motion through the ISM (Cheng 1983, Wang *et al.* 1993). However, based upon the space density of sources with similar brightness observed in the field, we do not consider the association between the pulsar and the faint residual source particularly compelling.

## 3. TIMING STUDIES

Using events extracted from a 30 arcsec (radius) circle centered on the source, we have searched for evidence of pulsations at the known radio period of 156 ms. While excluding $\sim 20 - 30\%$ of the source counts due to the finite spatial resolution of the mirror/PSPC system (the 90% fractional encircled energy radius ranges from $\sim 35$ arcsec at 0.3 keV to $\sim 50$ arcsec at 1.7 keV), this smaller source region reduces the background by a factor of $> 30$ over that in the 2.5 arcmin circle used for determining the source strength, providing increased sensitivity for the detection of pulsations. Event times were propagated to the solar system barycenter using the radio pulsar coordinates, and the $Z_n^2$ test (Buccheri *et al.* 1983) was used to search for modulation at the fundamental and first harmonic frequencies:

$$Z_n^2 = \frac{2}{N} \sum_{k=1}^{n} \left[ \left( \sum_{j=1}^{N} \cos k\phi_j \right)^2 + \left( \sum_{j=1}^{N} \sin k\phi_j \right)^2 \right] \qquad (1)$$

where $N$ is the total number of counts, $\phi_j$ is the phase associated with event time $t_j$ (relative to the period being tested), and $n$ is the number of harmonics being considered. A

recent radio ephemeris (Table 2) spanning the observation interval was obtained from the pulsar database maintained by the pulsar group at Princeton (as described by Taylor *et al.* 1993). We find no evidence for pulsations at the expected frequency, although the limited number of counts ($N = 61$) does not provide a high detection sensitivity. An upper limit to the pulsed power can be established based upon the $Z_n^2$ statistic (van der Klis 1989). For the first harmonic, the pulsed power is

$$f = 2\sqrt{\frac{(Z_1^2/2) - 1}{N}}. \tag{2}$$

Since, for random event times, $Z_1^2$ is distributed as $\chi^2$ for two degrees of freedom, the null detection permits us to establish a $3\sigma$ upper limit $f \lesssim 50\%$. The expected number of background counts in the 30 arcsec circle is $\sim 16$. Thus, the pulsed power from the pulsar alone is $\lesssim 77\%$. This value is clearly not very constraining; with the exception of the Crab pulsar, which is nearly 100% pulsed, most pulsars have pulsed components smaller than the upper limit derived for PSR 0355+54. Similar analysis for X-rays from PSR 1055–52, for example, reveals a broad-band pulsed component of $\sim 8\%$. This component increases to $\sim 85\%$ when only higher energy ($E \gtrsim 0.5$ keV) photons are considered (see Ögelman and Finley 1993), but a corresponding effect in PSR 0355+54 would not be seen due to lack of photons.

## 4. SPECTRAL STUDIES

The PSR 0355+54 spectrum was extracted from a circular region of radius 2.5 arcmin, with background determined from the surrounding annulus extending to 4.2 arcmin. The limited number of photons precludes attempts at spectral fitting to characterize the X-ray emission. However, by considering the number of counts in broad energy bands, it is possible to calculate hardness ratios which provide considerable information about the spectrum. We have used the binning scheme adopted in the IRAF/PROS analysis software and have tabulated counts in the following bands (corresponding to those used in the PSPC standard processing): A ($11 \leq$ PI $\leq 41$), B ($52 \leq$ PI $\leq 201$), C ($52 \leq$ PI $\leq 90$), and D ($91 \leq$ PI $\leq 201$); corresponding PROS bin boundaries are 3–10 (A), 13–30 (B), 13–18 (C), and 19–30 (D). We then calculated the hardness ratios

$$H_1 = \frac{(B-A)}{(B+A)} = 0.51 \pm 0.40$$

$$H_2 = \frac{(D-C)}{(D+C)} = 0.74 \pm 0.30. \tag{3}$$

Using the same event selection criterion, we have calculated the hardness ratios for PSR 1055–52: $H_1 = -0.81 \pm 0.01$, $H_2 = -0.58 \pm 0.05$. Clearly the values for PSR 0355+54 suggest a spectrum which is either inherently harder than that of PSR 1055–52, or which is more strongly absorbed.

We have carried out a spectral fit for PSR 1055–52 using data from both the ROSAT PSPC and the *Einstein* IPC. We find the best fit for a two-component model (blackbody plus power law) with the parameters listed in Table 3; the temperature and power law index are in good agreement with those determined by Ögelman and Finley (1993) using only PSPC data plus the additional constraint that the power law index conform within $2\sigma$ to that derived from the GRO data; our determination of the relative contribution between the two components differs somewhat, however. Using the best-fit value for $N_H$, we have estimated the column density for PSR 0355+54 by scaling this to the ratio of dispersion measures ($N_H = 6.1 \times 10^{20}$ cm$^{-2}$). We then folded the PSR 1055–52 model spectrum through the additional absorption to determine whether the difference in hardness ratios was an artifact of the column density. The hardness ratios for PSR 0355+54 are not reproduced by this process; the model spectrum is still considerably softer than that observed. However, the ISM ionization fraction toward PSR 1055–52 is likely to be much higher than that toward PSR 0355+54; with a dispersion measure of 30 cm$^{-3}$ pc (Taylor *et al.* 1993), the $N_H$ value for PSR 1055–52 derived from the X-ray data yields an ionization fraction of 0.22 which is in the upper range of expected values.

The value of $N_H$ for PSR 0355+54 has been measured directly from 21 cm absorption observations (Gómez-Gonzàlez and Guélin 1974). Absorption features are observed over a velocity range $\sim 0$ to $-25$ km s$^{-1}$ with optical depths $\tau < 0.15$ for an integrated total absorption $\int \tau \, dv = 11$ km s$^{-1}$. Assuming a hydrogen spin temperature $T_s = 100$K, this yields $N_H = 2 \times 10^{21}$ cm$^{-2}$. Adopting this value with the spectral model for PSR 1055–52 yields hardness ratios closer to that observed for PSR 0355+54 , though still somewhat softer than the observed values. Gómez-González and Guélin (1974) note that the 21-cm measurement for PSR 0355+54 was carried out at low resolution, so that the quoted total absorption is actually an underestimate. Increasing the $N_H$ value somewhat over that derived above brings the model hardness ratios more into line with those observed, but still predicts a spectrum softer than that observed, possibly suggesting a weaker low-temperature thermal component than that for PSR 1055–52.

With the limited spectral information available, we can still consider two important scenarios for the emission from PSR 0355+54 which will help characterize the emission. We first consider the possibility that the X-ray flux is associated with thermal emission from the entire NS surface, as might be expected from cooling of the interior. We will show that

this does not seem likely based upon the available data. Then we will derive the X-ray luminosity assuming Crab-like parameters for the emission, and investigate the associated X-ray luminosity in terms of the available spin-down power.

### 4.1. Blackbody Emission

After core collapse in a Type II supernova, a NS forms with an interior temperature of $\sim 10^{11} - 10^{12}$ K. Initial cooling proceeds rapidly through neutrino emission from the core, primarily generated through the direct URCA reactions. Subsequent cooling depends sensitively on the core equation of state as well as on the structure of the NS crust where neutrino bremsstrahlung may be important. As energy diffuses to the NS surface, it is radiated as blackbody emission with a characteristic temperature of $10^5 - 10^6$ K, peaking in the soft X-ray band. X-ray studies thus provide the most sensitive probe of NS cooling and the star's internal structure, including 1)the possibility that the direct URCA process operates at lower temperatures (and, thus, later times) due to large central densities (Lattimer *et al.* 1992, Page and Applegate 1992); 2)reheating due to frictional coupling of the crust and a separately rotating superfluid component (Shibazaki and Lamb 1989); 3)presence of exotic matter in the NS core (Shibazaki and Lamb 1989, Page and Baron 1990); 4)effects of superfluidity in the NS crust (Nomoto and Tsuruta 1987, Shibazaki and Lamb 1989); and 5)the possibility of crust bremsstrahlung suppression due to band structure effects (Pethick and Thorsson 1994). Observations of cooling neutron stars have been reviewed recently by Ögelman (1994) who finds that the most convincing cases for cooling do not require the extended direct URCA cooling, nor do they suggest the presence of exotic material in the core which would lead to rapid cooling.

To investigate such scenarios for the emission from PSR 0355+54, we have considered emission from the entire surface of a NS with $R = 10$ km. This scenario is consistent with the lack of observed pulsations, although the limit derived for the pulsed fraction is not particularly constraining in this regard. To derive an effective surface temperature which, given the characteristic age of the pulsar, may be compared with cooling models, we assume a column density $N_H = 2 \times 10^{21}$ cm$^{-2}$ derived from 21-cm absorption measurements. For a distance of 2.1 kpc (Taylor *et al.* 1993), a blackbody temperature $kT = 82 \pm 4$ eV ($T = 9.5(\pm 0.5) \times 10^5$ K) is required to produce the observed PSPC count rate. This yields a luminosity $L_x(0.1 - 2.4 \text{ keV}) = 5.7 \times 10^{32}$ erg s$^{-1}$. The corresponding surface temperature, when corrected for gravitational redshift assuming a 1.4 $M_\odot$ NS of radius 10 km (Helfand *et al.* 1980) is $kT = 108 \pm 5$ eV ($T = 1.25(\pm 0.07) \times 10^6$ K).

A thermal spectrum emitted from the NS surface will undergo modification in the

presence of an atmosphere (Miller 1992, Shibanov *et al.* 1992) which may result in an enhancement of the Wein tail of the blackbody spectrum (at the expense of the Rayleigh-Jeans region). The effective temperature derived from the modified spectrum may vary considerably from that of a pure blackbody; Ögelman and Finley (1993) find nearly a factor of two difference in the effective temperature for a Shibanov *et al.* (1992) model when comparing it to an unmodified blackbody using PSR 1055–52 data obtained with the ROSAT PSPC. Similar calculations by Miller (1992) predict a somewhat smaller effect for ROSAT HRI observations. The effect is dependent upon both the magnetic field strength and the NS surface temperature and composition. The derived effective temperature further depends upon the spectral response of the detectors; if the effective area peaks where the spectrum is relatively unmodified, the derived temperature will be close to the actual surface temperature. Attempts at modeling the atmosphere effects are beyond the scope of this paper, and the number of photons collected, but inspection of previous results suggests that presence of an atmosphere would not change the derived temperature for PSR 0355+54 by as much as a factor of two.

The derived temperature falls above current cooling models (Figure 2). The data thus fail to constrain the models even though the derived temperature must be considered an upper limit since contribution from another emission component cannot be ruled out by the data; indeed, as we discuss below, the bulk of the emission appears to be derived from the pulsar spin-down.

Since the blackbody normalization is set by the pulsar radius and distance, and we have also specified the value of $N_H$, the temperature is the only free parameter in the above analysis; the uncertainty in temperature reflects the uncertainty in the count rate. In reality, we have enough spectral information to confront this scenario more critically by considering the derived hardness ratios $H_1$ and $H_2$. Keeping the blackbody normalization fixed, we have considered a range of $N_H$ values and calculated the temperatures required to produce the observed count rate. We then generated models of these spectra, folded them through the PSPC spectral response, and calculated the associated hardness ratios. We find that blackbody emission from the entire surface, for any reasonable $N_H$ values, cannot reproduce the observed hardness ratios (Figure 3); the observed spectrum is harder than can be accommodated with thermal emission from the entire surface. We note, however, that thermal emission from a hot polar cap is not ruled out by these measurements (see Section 5). We also find that accretion from the ISM cannot account for the observed luminosity (see Section 5). We conclude that the emission is primarily associated with either the pulsar magnetosphere or a compact synchrotron nebula; in either case, it is derived primarily from the pulsar's spin-down power. This indicates that the above temperature must be

considered a strong upper limit; more sensitive observations are needed to define better the spectrum in order to assess the contribution of cooling to the total X-ray flux.

### 4.2. Power Law Emission

X-rays associated with energy derived from the pulsar magnetosphere can be produced in several ways. A relativistic electron wind may be confined by the ambient circumstellar magnetic field, resulting in a synchrotron nebula such as those associated with the Crab and Vela pulsars. Alternatively, direct magnetospheric X-rays can be produced in polar or outer gap regions where charge depletion allows strong **E** fields to develop along the NS magnetic field lines.

In outer gap models, high energy radiation is produced through a bootstrap mechanism whereby energetic primary electrons generate $\gamma$-rays which, in turn, result in a pair-production cascade; the secondary electrons boost ambient photons to high energies through inverse Compton scattering. Heating of the polar cap from backflow of relativistic electrons may produce soft X-ray emission. The magnetosphere can be classified as "Crab-like" or 'Vela-like" based upon whether curvature radiation or inverse Compton scattering is the dominant initial mechanism (Cheng, Ho, and Ruderman 1986a,b). A "death line" for the outer gap mechanism can also be derived (Chen and Ruderman 1993) based upon the values of $P$ and $B$ (Figure 4). The $\gamma$-ray production efficiency $L_\gamma/\dot{E}$ increases as pulsars approach this death line.

In polar cap models (e.g. Daugherty and Harding 1982) curvature radiation in polar cap gap regions is responsible for the $\gamma$-ray production. Bombardment of the polar caps results in heating and soft X-ray production. This scenario has been proposed to explain X-ray and $\gamma$-ray results from Geminga (Harding *et al.* 1994), and may explain the relatively hard emission from PSR 0355+54 .

PSR 0355+54 falls just below the death-line for outer-gap emission, as do several isolated X-ray emitting pulsars, though this line is actually somewhat dependent upon the inclination between the **B**-field and the rotation axis. PSR 1055–52 also falls just below the death-line; X-ray and $\gamma$-ray emission suggest this source may actually operate under Vela-like acceleration conditions. This suggests the strong possibility that PSR 0355+54, like PSR 1055–52, could be an observable $\gamma$-ray source.

To investigate the characteristics of any power-law emission, we have assumed a Crab-like spectrum (photon index $\alpha = 2$) and $N_H = 2 \times 10^{21}$ cm$^{-2}$, as before. For such a spectrum, we find an X-ray luminosity $L_x(0.1 - 2.4 \text{ keV}) = 1.0 \times 10^{32}$ erg s$^{-1}$. This is

consistent with observed luminosities for other pulsars (Figure 5). In particular, it is very similar to that which we derive for the power-law component from PSR 1055–52; using the PSR 1055–52 spectral index of 1.5 (see Table 3) reduces the PSR 0355+54 luminosity by a factor of two. The PSR 0355+54 results are in good agreement with other spin-down correlations, which further supports the interpretation of nonthermal emission.

## 5. DISCUSSION

The prospect of accretion from the ISM as the source of the X-ray luminosity has been discussed by Treves and Colpi (1991). The measured proper motion for PSR 0355+54 is $\sim 8$ mas yr$^{-1}$ (Lyne *et al.* 1982). For a distance of 2.1 kpc, this provides a velocity lower limit $v \geq 30$ km s$^{-1}$. For spherically symmetric accretion, the accretion rate for a star moving through the ISM is (Bondi and Hoyle 1944; see Helfand *et al.* 1980)

$$\dot{M} = 3.73 \times 10^8 \left(\frac{M}{M_\odot}\right)^2 n_{\rm H} v_{100}^{-3} \tag{4}$$

where $n_{\rm H}$ is number density of the ambient medium and $v_{100}$ is NS velocity in units of 100 km s$^{-1}$. Assuming a mass conversion efficiency $\dot{E} = 0.1\dot{M}c^2$, typical of values derived for accretion onto a NS in binary systems, this yields $L_x = 2 \times 10^{30}$ erg s$^{-1}$ for $n_{\rm H} = 1$ cm$^{-3}$, which is more than twice the average value assuming the values of $N_H$ and $D$ used above; an increase of $n_{\rm H}$ by two orders of magnitude would be required to yield the observed luminosity, which seems quite unreasonable.

We have shown that the hardness ratios derived from the PSR 0355+54 data are not consistent with thermal emission from the entire NS surface, and have thus concluded that the bulk of the emission can not be attributed to cooling of the NS interior. A thermal spectrum at higher temperature, with a corresponding reduction in the size of the emitting region, is a distinct possibility, however. Such a scenario is expected in both polar and outer gap models due to heating of the polar caps by streams of energetic particles, and such a model has been proposed to describe X-ray data from PSR 1929+10 (Yancopoulos *et al.* 1994). For an aligned dipole field, the size of the polar cap is defined by the last closed field line:

$$r_{\rm cap} = \sqrt{\left(\frac{2\pi R^3}{cP}\right)}. \tag{5}$$

We may thus use the PSR 0355+54 period to calculate an emitting area for the polar cap in an aligned rotator: $A = 4.3 \times 10^9$ cm$^2$. Along with the distance, this defines the normalization for a model of blackbody emission from the polar caps. In order to reproduce

the observed count rate, again assuming $N_H = 2 \times 10^{21}$ cm$^{-2}$, the cap temperature (corrected for redshift) must be $kT = 301.6$ eV ($T = 3.5 \times 10^6$ K). A model spectrum with these parameters again fails to reproduce the observed hardness ratios, although it provides a better representation than can be accomplished with models for emission from the entire surface; it may indeed be possible to reproduce the results with proper combinations of $A$, $T$, and $N_H$, but the data are not sufficient to permit such independent determinations. In Figure 3 we plot hardness ratios derived for blackbody models with with $N_H$ fixed as above, and with temperature and emitting area varying so as to produce the observed count rate for PSR 0355+54 . We note that the temperature derived above is very similar to that found for apparent polar cap emission from PSR 1929+10 (Yancopoulos *et al.* 1994).

For a nearly orthogonal dipole, the X-ray luminosity resulting from bombardment of the polar caps is (Arons 1981a, Harding *et al.* 1994)

$$L_x \approx 4 \times 10^{26} \mu_{30} P^{-27/8} \text{ erg s}^{-1} \tag{6}$$

where $\mu_{30}$ is the pulsar magnetic dipole moment in units of $10^{30}$ G cm$^3$. For PSR 0355+54, this predicts a luminosity $L_x \approx 10^{29}$ erg s$^{-1}$ which is considerably smaller than the observed luminosity. Additional heating associated with positron trapping (and subsequent acceleration toward the poles) in the weak-field outer regions of the magnetosphere may increase the luminosity to $\sim 10^{31}$ erg s$^{-1}$ (Arons 1981b), still too small to agree with the observations; further, this mechanism may only be applicable to slow pulsars with relatively small fields. It would appear that, if polar cap emission is indeed responsible for the X-ray emission, the associated particle acceleration does not occur (at least uniquely) in the polar regions.

As shown in Figure 5, the luminosity derived for PSR 0355+54 corresponds well to that of other isolated pulsars based upon the available spin-down power. The solid lines indicated in the figure correspond to $L_x = \dot{E}$ and

$$L_x = 2.5 \times 10^{-17} \dot{E}^{1.39} \tag{7}$$

an empirical relationship derived by Seward and Wang (1988) based upon *Einstein* results; Ögelman (1994) finds a similar result based upon more recent ROSAT pulsar detections. In the Figure, we have indicated the luminosity of the power law component only for PSR 1055–52 (see Table 3). This value is in excellent agreement with the derived luminosity for PSR 0355+54, as one might expect given the similarity in parameters, and gives further indication that the observed emission is derived from the spin-down.

In PSR 1055–52, the power law component appears to extend from the X-ray to the $\gamma$-ray range; the spectral values given in Table 3 predict a $\gamma$-ray

flux $F(E > 100\ \mathrm{MeV}) = 4.1 \times 10^{-7}$ photons cm$^{-2}$ s$^{-1}$, in reasonable agreement with the observed value of $2.7(\pm 0.5) \times 10^{-7}$ photons cm$^{-2}$ s$^{-1}$. This suggests an association between the emission mechanisms which might be expected to hold for PSR 0355+54 . Assuming the same power law index leads to a predicted $\gamma$-ray flux $F(E > 100\ \mathrm{MeV}) = 1.9 \times 10^{-7}$ photons cm$^{-2}$ s$^{-1}$. Clearly there are mitigating factors, such as magnetic field orientation and geometry, which make such an estimate quite uncertain. Current limits on emission from PSR 0355+54 derived from *EGRET* data are (Thompson *et al.* 1994) $F(E > 100\ \mathrm{MeV}) = 2.8 \times 10^{-7}$ photons cm$^{-2}$ s$^{-1}$ and $F(E > 1\ \mathrm{GeV}) = 2.4 \times 10^{-8}$ photons cm$^{-2}$ s$^{-1}$. Based upon the X-ray luminosity and known $\gamma$-ray behavior of PSR 1055–52, it appears extremely worthwhile to pursue further $\gamma$-ray studies of PSR 0355+54 .

The author would like to thank H. Ögelman, M. C. Miller, and A. Harding who all provided helpful insight in interpreting the results. Thanks also to D. Helfand whose comments and suggestions, as referee, helped clarify and strengthen many portions of the text. This work was supported by the National Aeronautics and Space Administration through grant NAG5-2329, and contract NAS8-39073.

Table 1

Pulsar parameters for PSR 0355+54 and PSR 1055–52

| PSR | $P$ (ms) | $\dot{P}/10^{-15}$ ( s $s^{-1}$) | $\log \dot{E}$ (erg $s^{-1}$) | $\log T$ (years) | DM ($cm^{-3}$ pc) | D (kpc) | $\log B$ (Gauss) |
|---|---|---|---|---|---|---|---|
| 0355+54 | 156 | 4.4 | 34.66 | 5.75 | 57 | 2.07 | 11.92 |
| 1055–52 | 197 | 5.8 | 34.48 | 5.73 | 30 | 1.53 | 12.04 |

Table 2

PSR 0355+54 Pulse Ephemeris

| Parameter | Value |
|---|---|
| $P$(s) | 0.15638220635 |
| $\dot{P}$(s $s^{-1}$) | $4.39659 \times 10^{-13}$ |
| $T$(JD) | 2449060.0 |

Table 3

PSR 1055–52 Fit: Blackbody + Power-Law

| Component | Parameter[a] | Value[b] |
|---|---|---|
| Blackbody | $kT$(keV) | $61.8 \pm 4.2$ |
| | $F_x$ (erg $cm^{-2}$ $s^{-1}$) | $2.3 \times 10^{-12}$ |
| Power Law | $\alpha$ | $1.5 \pm 0.7$ |
| | $F_x$ (erg $cm^{-2}$ $s^{-1}$) | $2.3 \times 10^{-13}$ |

a) Flux evaluated in 0.1–2.4 keV energy band

b) For comparison, Ögelman and Finley (1993) find $F_{BB} = 1.1 \times 10^{-11}$ and $F_{PL} = 4.8 \times 10^{-14}$

## REFERENCES


Alpar, M. A., Pines, D., & Cheng, K. S. 1988, Nature, 348, 707

Arons, J. 1981a, Ap J, 248, 1099

Arons, J. 1981b, in *Pulsars*, IAU Symposium No. 95, eds. W. Sieber and R. Wielebinski (Dordrecht:Reidel) p.69

Bondi, H. & Hoyle, F. 1944, MNRAS, 104, 273.

Brinkmann, W., & Ögelman, H. 1987, A&A, 182, 71

Buccheri, R. *et al.* 1983, A&A, 128, 245

Chen, K., & Ruderman, M. 1993, ApJ, 402, 264

Cheng, A. F. 1983, ApJ, 275, 790

Cheng, A. F., & Helfand, D. J. 1983, ApJ, 217, 271

Cheng, K. S., Ho, C., & Ruderman, M. 1986a, ApJ, 300, 500

Cheng, K. S., Ho, C., & Ruderman, M. 1986b, ApJ, 300, 522

Daugherty, J. K., & Harding, A. K. 1982, ApJ, 252, 337

Fierro, J. M. *et al.* 1993, ApJ, 413, L27

Finley, J. P. 1994, to appear in Proceeding of the ROSAT Science Symposium.

Gómez-Gonzàlez, J., and Guélin, M. 1974, A&A, 32, 441

Harding, A. K., Ozernoy, L. M., & Usov, V. V. 1994, MNRAS, in press.

Helfand, D. J. 1983, in *Supernova Remnants and Their X-Ray Emission*, IAU Symposium 101, ed. J. Danzinger and P. Gorenstein (Dordrecht:Reidel), p.471

Helfand, D. J., Channan, G. A., & Novick, R. 1980, Nature, 283, 337.

Lattimer, J. M. *et al.* 1991, Phys. Rev. Lett., 66, 2701

Lyne, A. G. 1987, Nature 326, 569

Lyne, A. G., Anderson, B., & Salter, M. J. 1982, MNRAS, 201, 503

Manchester, R. N., Taylor, J. H., & Juguenin, G. R. 1972, Nature Phys. Sci. 240, 74

McCulloch, P.M. *et al.* 1978, MNRAS, 183, 645

Miller, M. C. 1992, MNRAS, 255, 129

Morris, D.A. *et al.* 1981, A&A Supp. Ser., 46, 421

Nomoto, K., & Tsuruta, S. 1986, ApJ, 305, L19

Ögelman, H. 1994, to appear in Proceedings of September 1993 NATO ASI on "Lives of Neutron Stars" - Kemer, Turkey.

Ögelman, H., & Finley, J. P. 1993, ApJ, 413, L31

Page, D., & Applegate, J. H. 1992, ApJ 394, L17

Page, D., & Baron, E., 1990, ApJ 354, L17

Pethick, C. J., & Thorsson, V. 1993, Phys. Rev. Lett., submitted.

Pfeffermann, E. *et al.* 1986, SPIE Proceedings, 733, 519

Seward, F. D., & Wang, Z-R 1988, ApJ, 332, 199

Shibazaki, N., & Lamb, F. K., ApJ, 346, 808, 1989

Shibanov, Y. A. *et al.* 1992, A&A, 266, 313

Taylor, J. H., Manchester, R. N., & Lyne, A. G. 1993, ApJ Supp., 88, 529

Thompson, D. J. 1994, ApJ - submitted.

Treves, A. & Colpi, M. 1991, A&A, 241, 107

van der Klis, M. 1989, in *Timing Neutron Stars*, Proceedings of the NATO ASI on Timing Neutron Stars, eds. H. Ögelman and E. P. J. van den Heuvel (Dordrecht:Kluwer), p.27

Wang, Q. D., Li, Z-Y., & Begelman, M. C. 1993, Nature, 364, 127

Yancopoulos, S., Hamilton, T. T., & Helfand, D. J. 1994, ApJ, submitted.

## FIGURE CAPTIONS

**Figure 1:** Contour plot of the X-ray emission from PSR 0355+54 (center). Contours are spaced at intervals of 20% of the pulsar peak emission. Inset image shows point source data from 3C 273, scaled to PSR 0355+54 flux levels. Images have been background-subtracted and smoothed with a 32 arcsec Gaussian profile.

**Figure 2:** Models for cooling of neutron star interior. References to models are given in text. Shibazaki and Lamb Model 1 is for standard cooling with no reheating (lower) and reheating due to frictional coupling between crust and superfluid core; Model 2 includes effects of pion condensates in core. Page and Baron models are for no superfluid, no exotic matter (upper) and superfluid with kaon condensates (lower). Nomoto and Tsuruta models contain no exotic core matter, and: superfluid (lower), and no superfluid (lower) for soft equation of state; no superfluid (middle) with stiff equation of state. Effective temperature at surface $T_s$ and at infinity $T_\infty$ for PSR 0355+54 is higher than all models, suggesting a spin-down origin for at least some fraction of the emission.

**Figure 3:** Hardness ratios derived for PSPC data for PSR 0355+54 . Connected points show hardness ratios derived for models of blackbody emission from surface of a neutron star with 10 km radius (squares), and for blackbody emission from a hot polar cap (triangle). Upper numbers correspond to temperature ($kT$ in eV), and lower numbers correspond to $\log N_H$ values (for squares – 21-cm value is indicated by box, and plot extends to 3 times this value to cover any reasonable values of $N_H$) or areas of emitting regions (triangles) required to produce observed number of source counts.

**Figure 4:** Magnetic field vs. rotation period for all pulsars. Death lines for Crab-like and Vela-like outer gap emission are indicated (after Cheng and Ruderman 1993). Known X-ray emitters are indicated. PSR 0355+54, like PSR 1055–52, lies at death line for Vela-like emission. In this region $\gamma$-rays dominate the outer gap emission, making PSR 0355+54 a good candidate for $\gamma$-ray study.

**Figure 5:** X-ray luminosity vs. spin-down power for known X-ray emitting isolated pulsars (after Seward and Wang 1988); luminosity values are from Ögelman (1994). PSR 0355+54 luminosity agrees well with other pulsar values, in particular that for the power-law component of PSR 1055–52, suggesting emission is derived from the pulsar spin-down.

PSR 0355+54

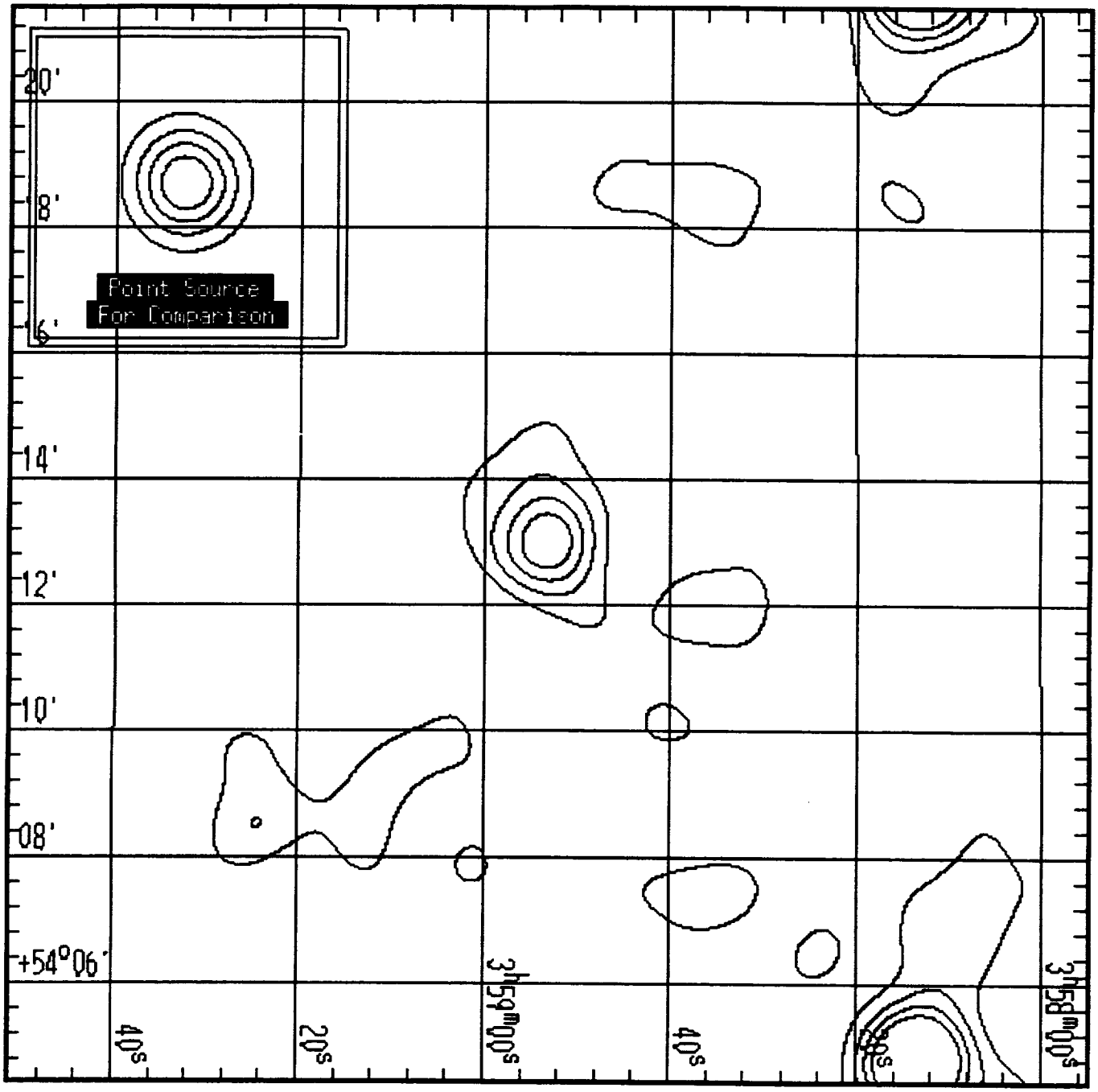


Fig. 1

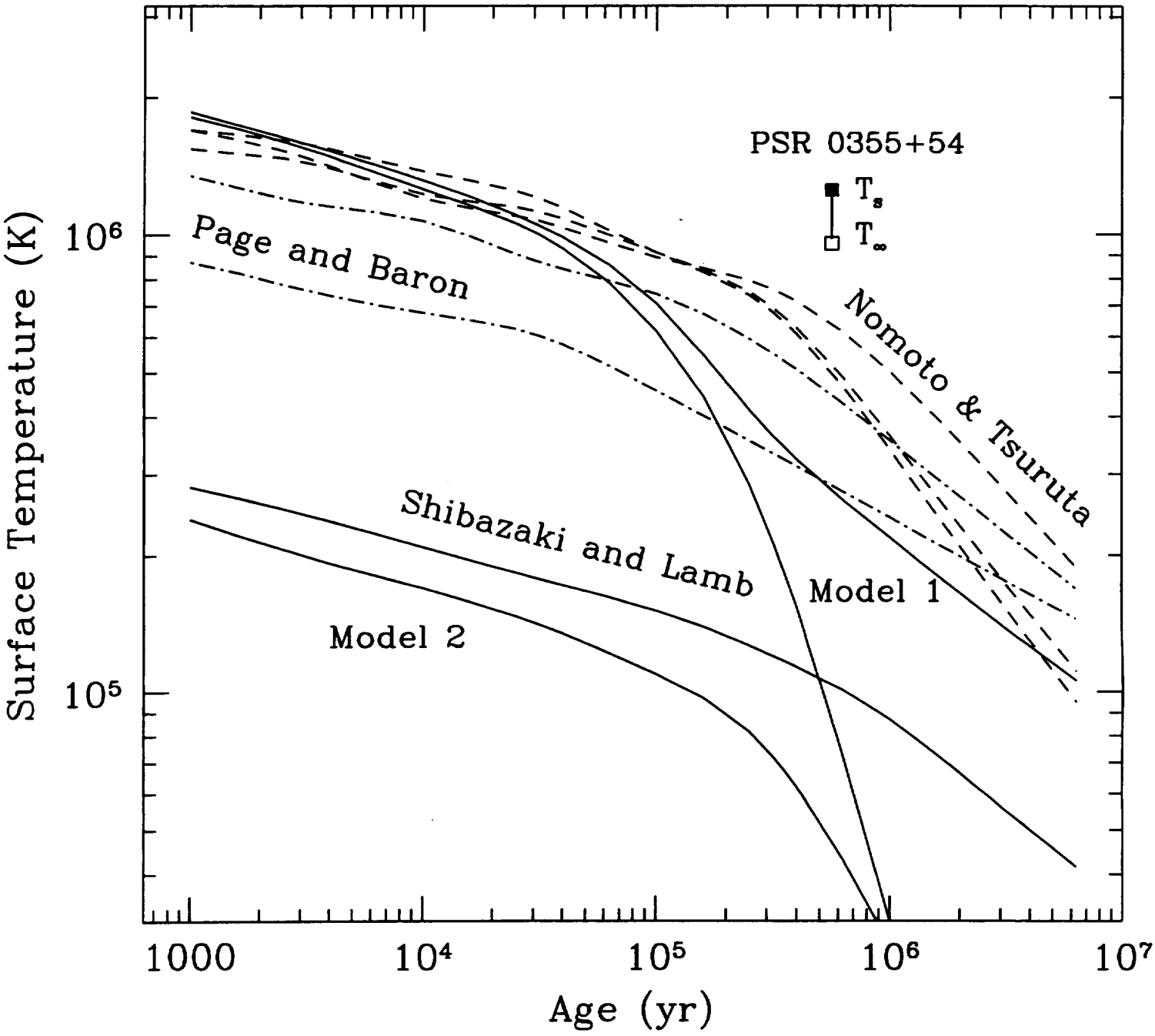
PSR 0355+54
$T_s$
$T_\infty$
Page and Baron
Nomoto & Tsuruta
Shibazaki and Lamb
Model 1
Model 2
Surface Temperature (K)
$10^6$
$10^5$
1000
$10^4$
$10^5$
$10^6$
$10^7$
Age (yr)

Fig. 2

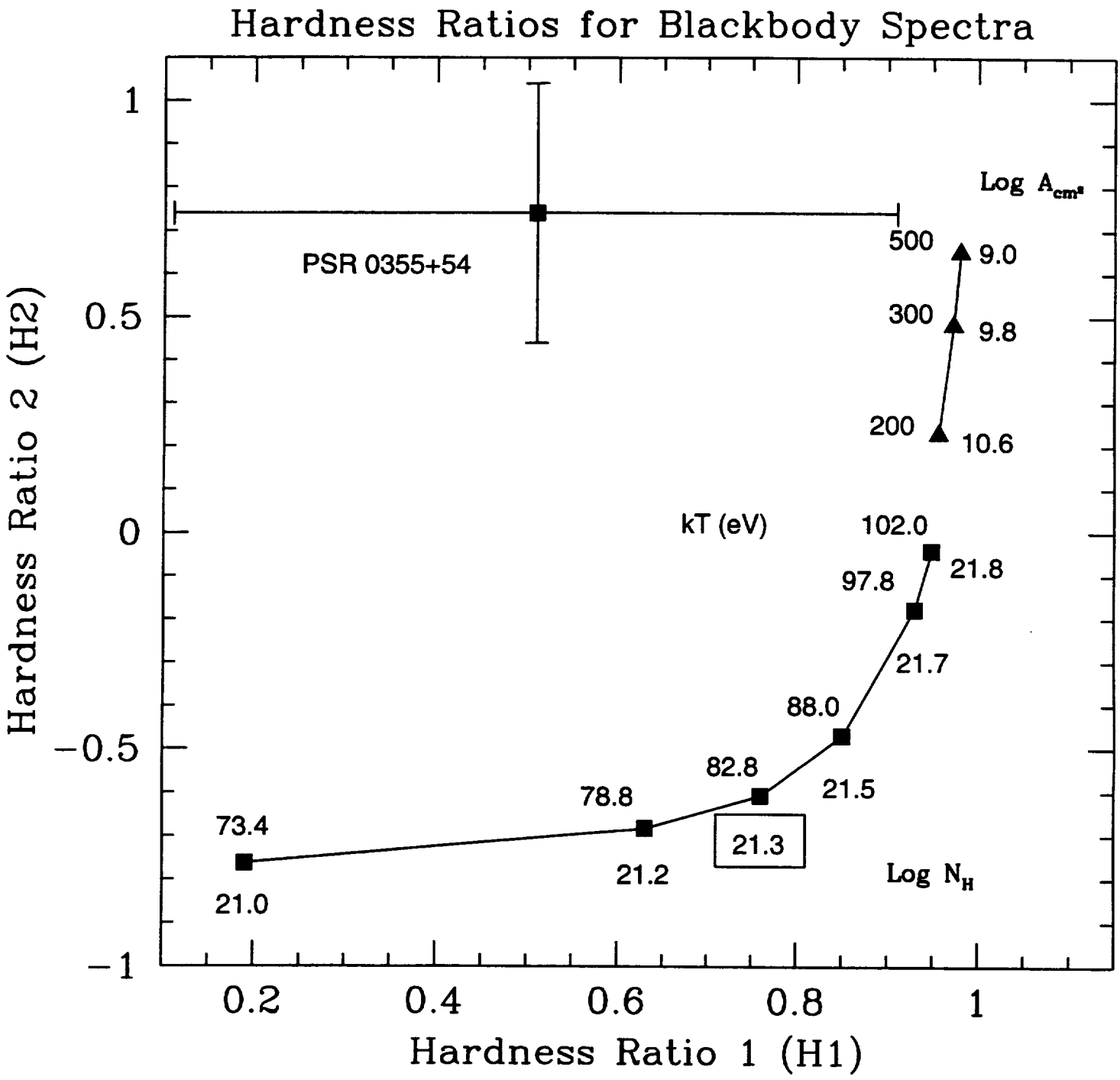
Hardness Ratios for Blackbody Spectra
Hardness Ratio 2 (H2)
Hardness Ratio 1 (H1)
1
0.5
0
−0.5
−1
0.2
0.4
0.6
0.8
1
PSR 0355+54
Log $A_{cm^2}$
500
9.0
300
9.8
200
10.6
kT (eV)
102.0
97.8
21.8
21.7
88.0
82.8
21.5
78.8
73.4
21.3
21.2
21.0
Log $N_H$

Fig. 3

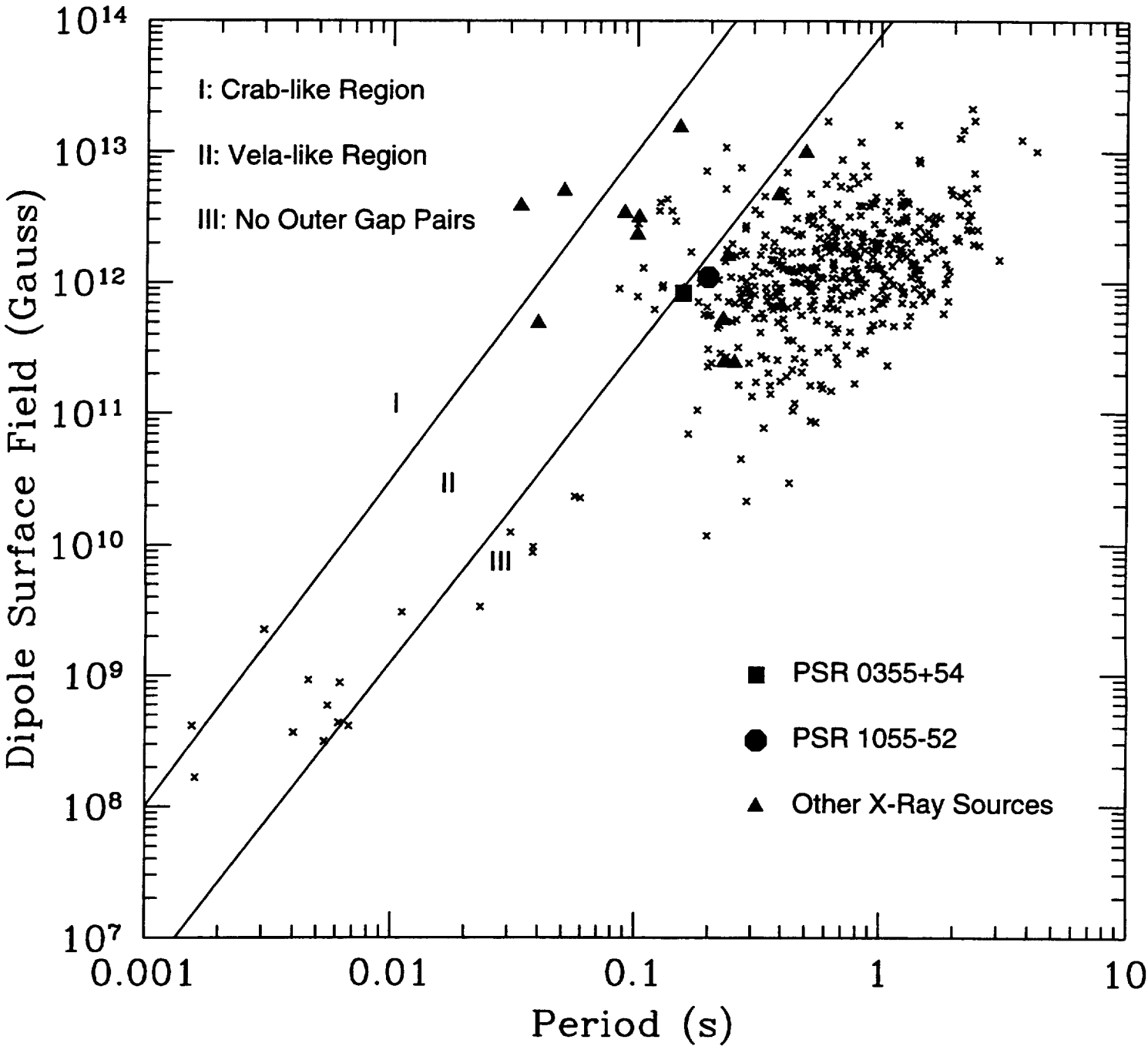
I: Crab-like Region
II: Vela-like Region
III: No Outer Gap Pairs
I
II
III
PSR 0355+54
PSR 1055-52
Other X-Ray Sources
Dipole Surface Field (Gauss)
Period (s)
$10^{14}$
$10^{13}$
$10^{12}$
$10^{11}$
$10^{10}$
$10^{9}$
$10^{8}$
$10^{7}$
0.001
0.01
0.1
1
10

Fig. 4

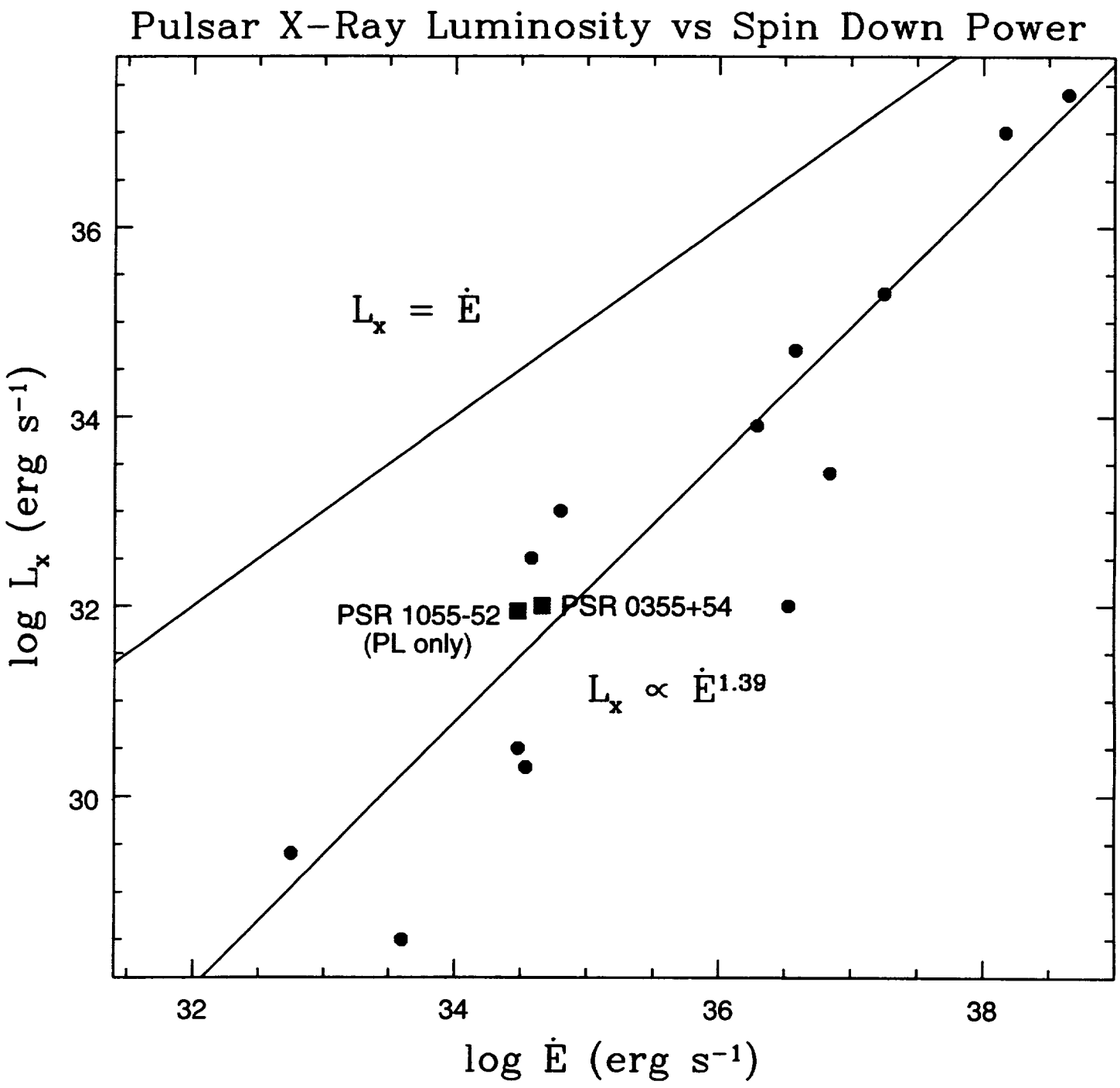
Pulsar X-Ray Luminosity vs Spin Down Power
$L_x = \dot{E}$
$L_x \propto \dot{E}^{1.39}$
PSR 1055-52
(PL only)
PSR 0355+54
log $L_x$ (erg $s^{-1}$)
log $\dot{E}$ (erg $s^{-1}$)
30
32
34
36
32
34
36
38

Fig. 5